Development of Shuttlecock Tumble and Smash Test Methods

SATHEESH KAVILADHIKARAKUNNATHU PUTHANVEETIL
VALERY CHERNORAY

Department of Mechanics and Maritime Sciences
CHALMERS UNIVERSITY OF TECHNOLOGY
Gothenburg, Sweden 2021

Project Report 2021

Development of Shuttlecock Tumble and Smash Test Methods

SATHEESH KAVILADHIKARAKUNNATHU PUTHANVEETIL
VALERY CHERNORAY

Department of Mechanics and Maritime Sciences
Division of Fluid Dynamics
Chalmers University of Technology
Gothenburg, Sweden 2021

Development of Shuttlecock Tumble and Smash Test Methods
SATHEESH KAVILADHIKARAKUNNATHU PUTHANVEETIL
VALERY CHERNORAY

Supervisor: Valery Chernoray, Department of Mechanics and Maritime Sciences

Project Report 2021
Department of Mechanics and Maritime Sciences
Division of Fluid Dynamics
Chalmers University of Technology
SE-412 96 Gothenburg
Telephone +46 31 772 1000

Typeset in LaTeX
Gothenburg, Sweden 2021

Development of Shuttlecock Tumble and Smash Test Methods
SATHEESH KAVILADHIKARAKUNNATHU PUTHANVEETIL
VALERY CHERNORAY
Department of Mechanics and Maritime Sciences
Chalmers University of Technology

Abstract

Feathered shuttlecocks are used in all type of high level competitions in badminton, however due to relatively high cost, low durability and due to less predictability involved in using bird feathers for its production, synthetic alternatives of shuttlecocks are being developed. BWF - Badminton World Federation, responsible for large tournaments like World Championships and the Olympics are interested in knowing how the characteristics of the new synthetic shuttlecocks is similar or different to that of traditional feathered ones so as to introduce synthetic shuttlecocks into the tournaments. Two major performance characteristics of a shuttlecock under consideration by BWF are tumbling or the erratic spinning of the shuttlecock at net play and smash resistance or the durability of the shuttlecock under repeated smash. Thus through this project, it was aimed to propose and evaluate test methods for comparing the performance of synthetic shuttlecocks during the process of tumbling and smash.

Keywords: Synthetic Shuttlecocks, Net spin, Tumble, Smash, Testing.

Acknowledgements

We would like to thank Mr. Ian Wright and Mr. Rodrigo Pacheco of BWF for funding of this project.

We would like to thank Mr. Christer Forsgren of Polyfor AB for giving us an opportunity to work in this interesting project and also for providing the right set of tools and information required from time to time.

We would also like to thank Mr. Isak Jonsson from the division of Fluid Dynamics in the development of various mechanisms used in this project, Mr. Edward Hadziavdic and Dr. Bercelay Niebles Atencio from the division of Fluid Dynamics for their help in the additive manufacturing of prototypes and Mr. Anil Kumar of the same division for his physical help in the smash tests.

Satheesh Kaviladhikarakunnathu Puthanveetil : Gothenburg, December 2020

Contents

Nomenclature

BWF	Badminton World Federation
COM	Center of Mass
FEM	Finite Element Method
g	Acceleration due to gravity
ORF	Observer Reference Frame
RRF	Racquet Reference Frame
SRF	Shuttlecock Reference Frame
V_A	Velocity Vector of the body A
V_B	Velocity Vector of the body B
V_{BA}	Relative Velocity of the body B with respect to body A
MARM	Mechanical Armed Release Mechanism
NTU	Nanyang Technical University
RISE	Research Institute of Sweden
SSLM	Smash using Spring Loaded Mechanism

1

Background

The previous iteration/phase was aimed at understanding the problem of testing tumbling and smash resistance. In order to achieve this initially an understanding of the badminton game was made followed by the understanding of its underlying components such as the design and design limitations of the shuttlecock and the racket, their general motion during a smash and tumble and a few of the underlying physics governing their motion. This understanding was then applied to develop working prototypes of a smash test rig and a tumble test rig, many concepts were created and their performances were compared, these will be discussed in the upcoming sections.

1.1 Release mechanisms

The development procedure required the creation of shuttlecock holding/ releasing mechanisms and two such mechanisms were introduced, one employed a mechanical arm powered by an electronic actuator which would grip the shuttle and release at will (refer figure 1.1), the next mechanism used vacuum to hold the shuttle cock and a electronically controlled pneumatic actuator was used to shoot the shuttle in the required direction, this mechanism is shown in figure 1.2

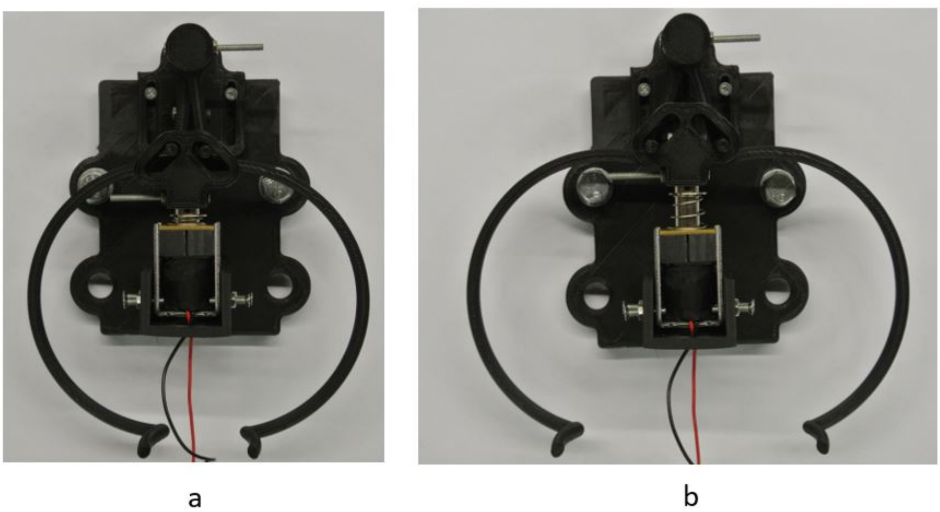

Figure 1.1: Mechanical armed shuttlecock release mechanism shown (a) without actuation and (b) with actuation.

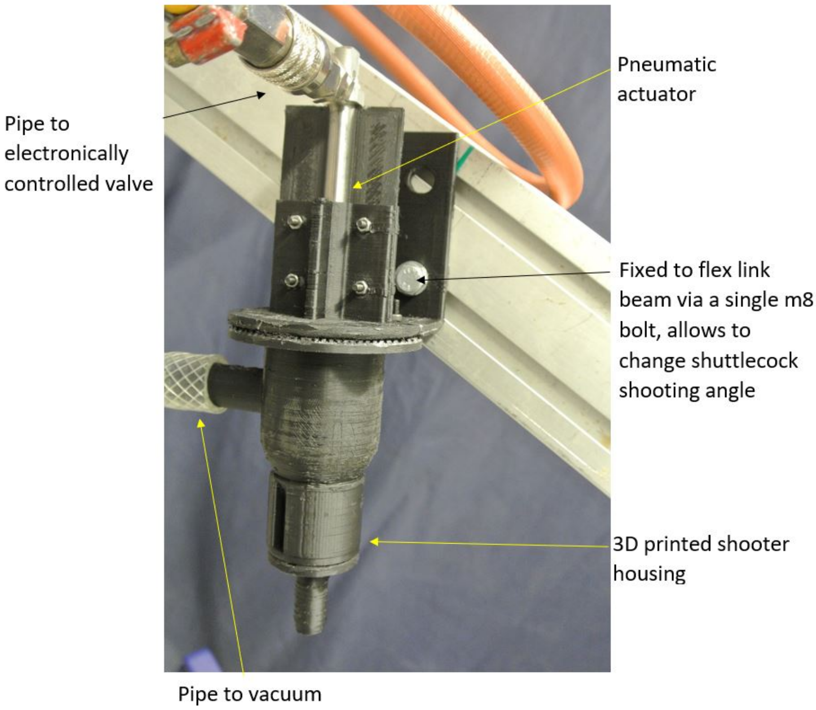

Figure 1.2: Pneumatic launcher - front portion.

1.2 Tumbling mechanisms

A look into the kinematics of tumbling motion showed that by using the idea of relative motion the complex motions can be simplified to achieve the same tumbling. The general principle of relative motion is depicted in figures 1.3 and 1.4. This ideology showed that the same tumbling process can be replicated in 3 way each of which gave a prototype:

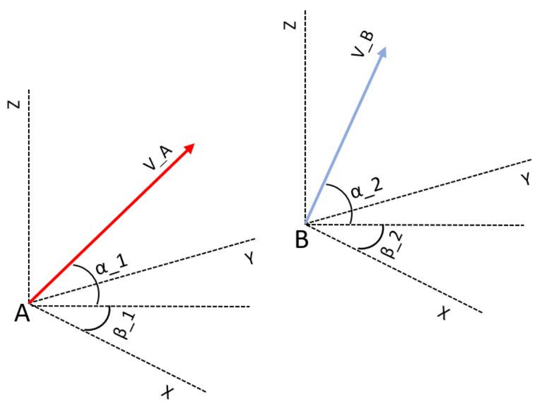

Figure 1.3: Velocity vectors of two bodies measured in the observer reference frame.

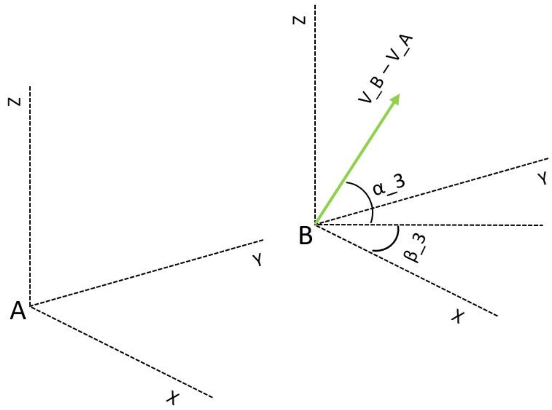

Figure 1.4: Relative velocity vector as seen from the reference frame of body A.

The first approach was to model the motion as in reality and to use a spinning racket powered by an electric motor while the shuttlecock was released by either of the 2 above mentioned release mechanisms, the prototype is shown in figure 1.5, this mechanism did produce tumbling however the synchronisation between the dropping shuttle and the spinning racket was proven to be difficult which meant that the shuttle missed the racket or impacted the racket at different positions when repeated, hence this mechanism was deemed less repeatable and discarded

The next approach was to fix the shuttle and impact it with a rod powered by the pneumatic actuator mechanism, this setup is shown in figure 1.6. However this device only produce little tumbling, in an attempt to increase the tumbling amount two other variation were tried where in one the shuttlecock was impacted at an angle, this increased the amount of tumble but only minimally. In the next variation a pin was added to the cork base of the shuttle and the impact was given at the pin tip and was thought to provide more torque to the shuttle despite which the mechanism did not improve the results as the pin increased the moment of inertia of the shuttle which compensated for the extra torque, the 3 variant are illustrated in figure 1.7

The final approach was to fix the racket at the desired orientation and shoot the shuttle with the pneumatic mechanism, this method created a realistic amount of tumble, it repeatability was better that the spinning racket mechanism but still had errors, however this was chosen as the best of the three in the previous iteration, this mechanism is shown in figure1.8

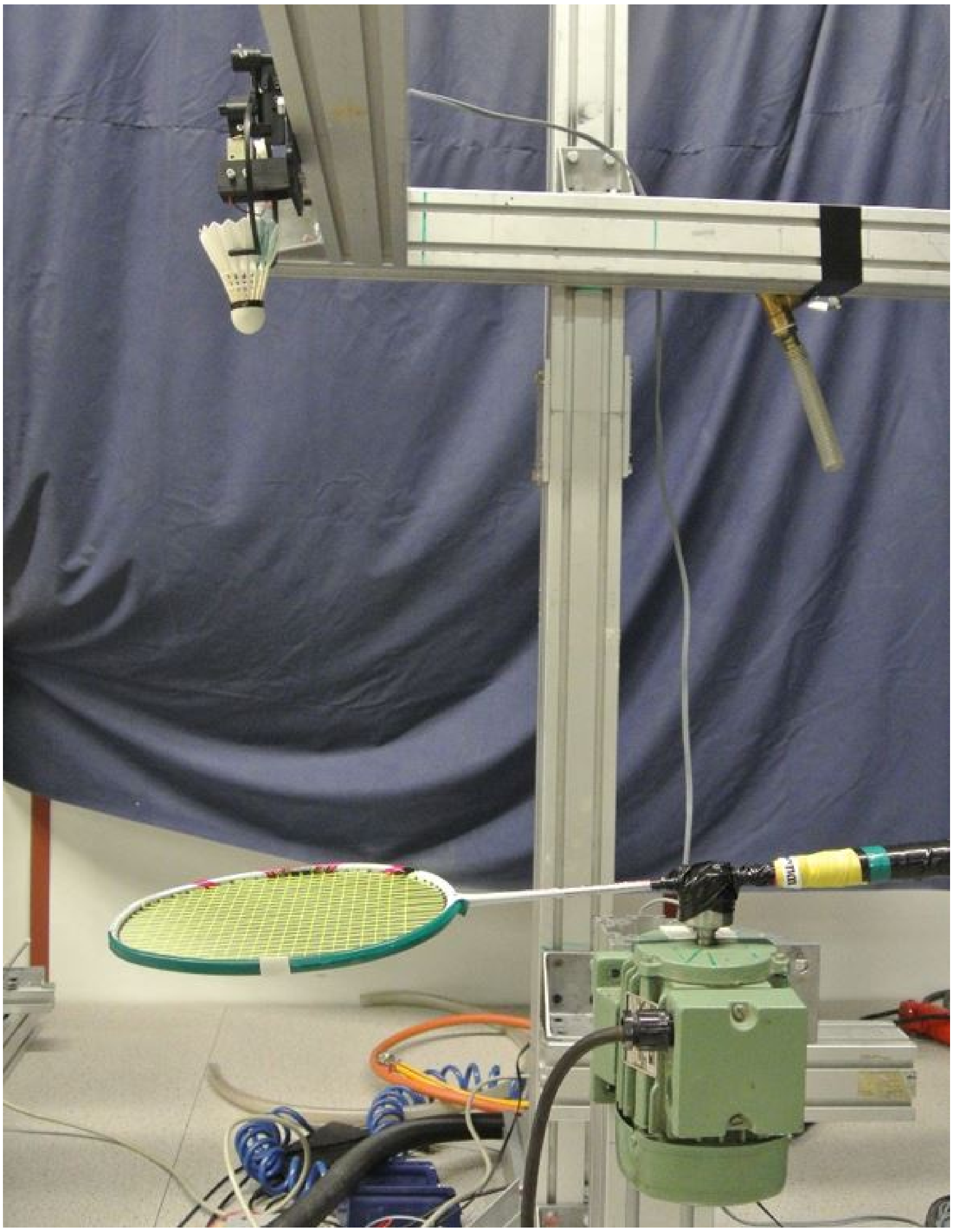

Figure 1.5: ORF - with mechanical arm shuttlecock release mechanism.

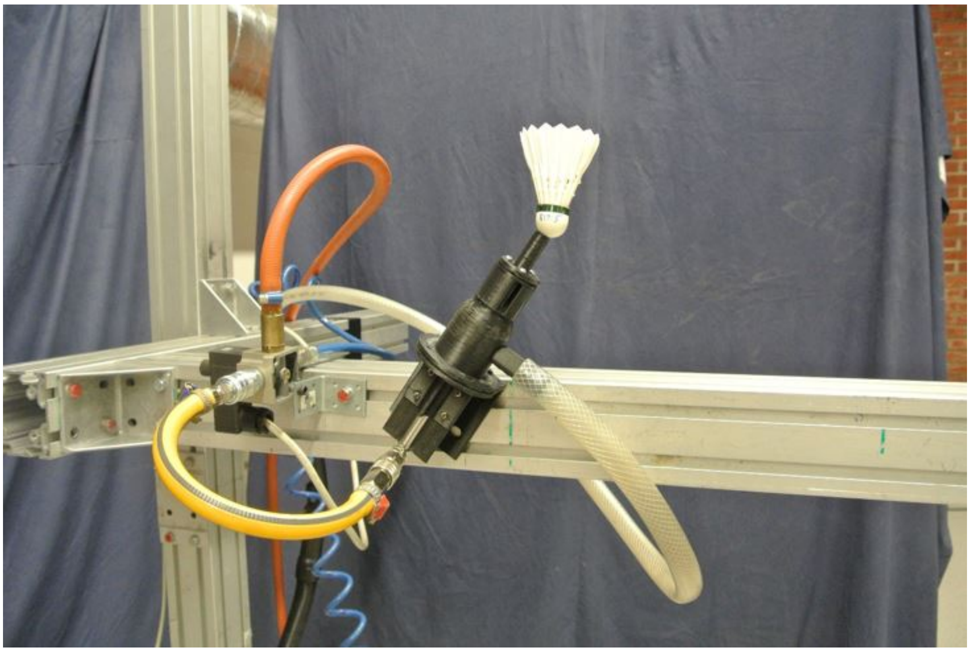

Figure 1.6: Side view of the experimental set up for replicating tumble from the Shuttlecock Reference Frame.

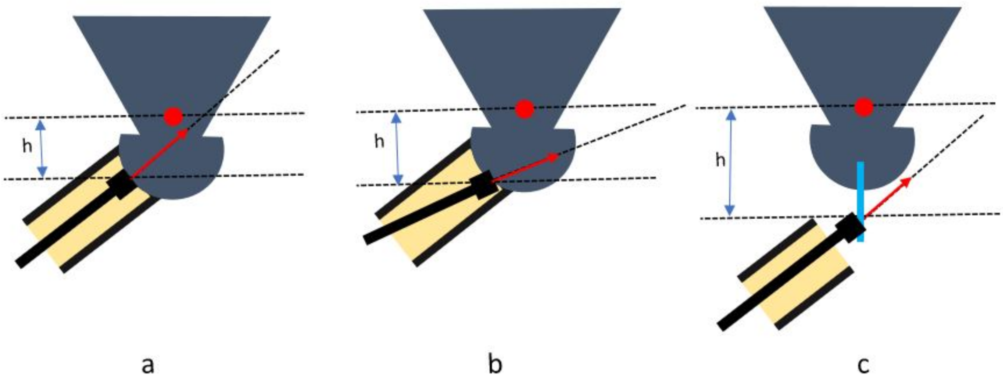

Figure 1.7: SRF experimental setup variants.

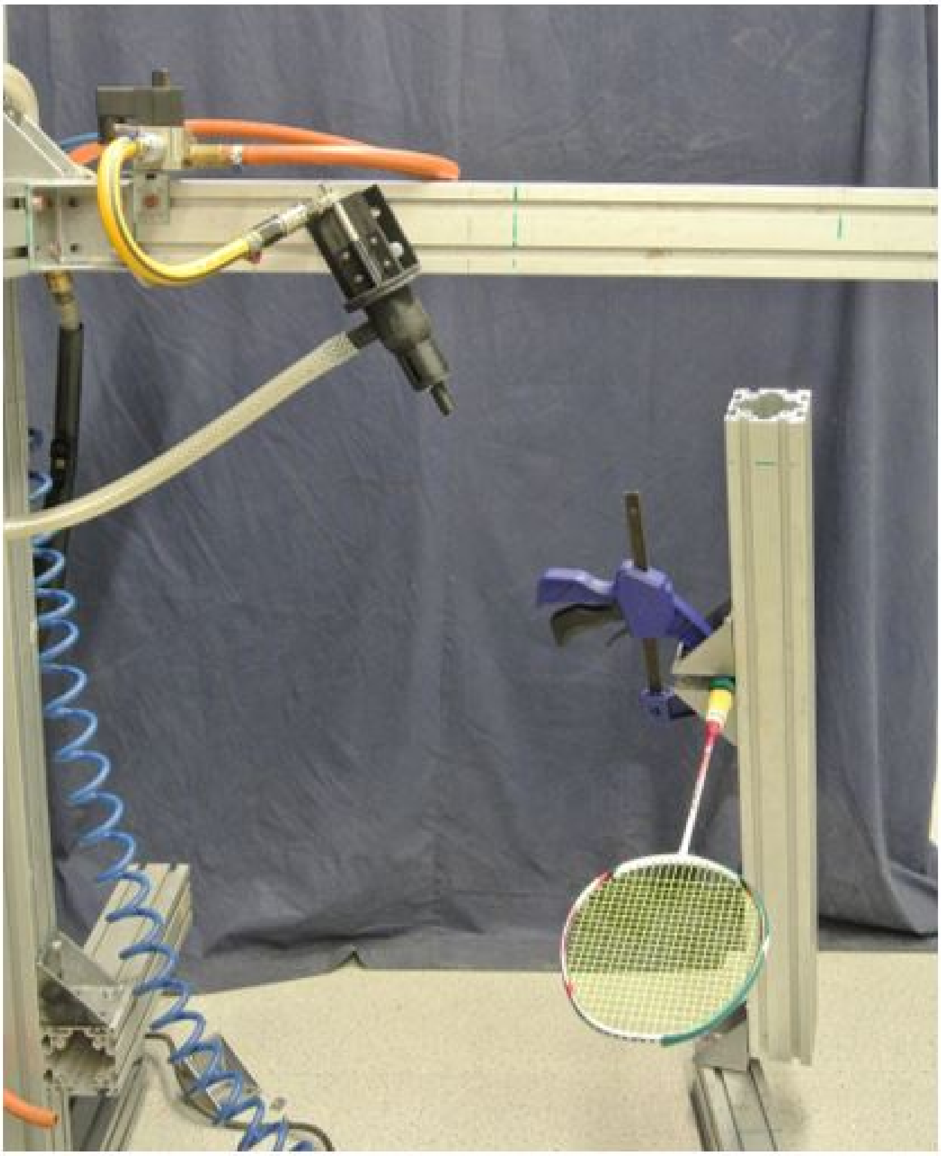

Figure 1.8: Front view of the experimental set up for replicating tumble from the racket Reference Frame.

1.3 Smashing mechanisms

Two mechanisms were produced and compared for smashing. One employed the use of a stiff bar made of carbon fiber, the racket was attached to the end of the bar, pulled back and released causing the bar to spring back and smashing the shuttle held in place by a drinking straw connected to a vacuum cleaner. This mechanism is shown in figure 1.9. This mechanism produced very less speed and it was also the least modifiable design hence it was discarded.

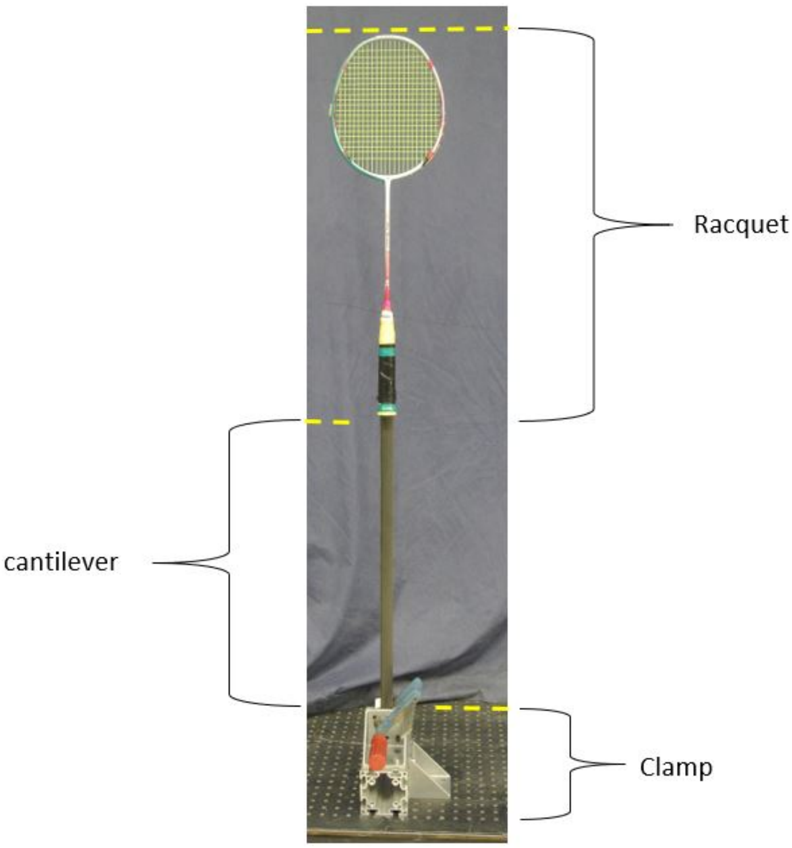

Figure 1.9: Front view of the experimental set up for replicating smash using cantilever mechanism.

The next design used the principle of an inverted pendulum, this mechanism was powered by spring and was modifiable. the mechanism is shown in figures 1.10 and 1.11, this design even though produced repeatable smashes it could only produce smash speeds of 25 m/s which was far less than the requirement, however it was chosen to proceed into the next phase as it was the better of the two designs.

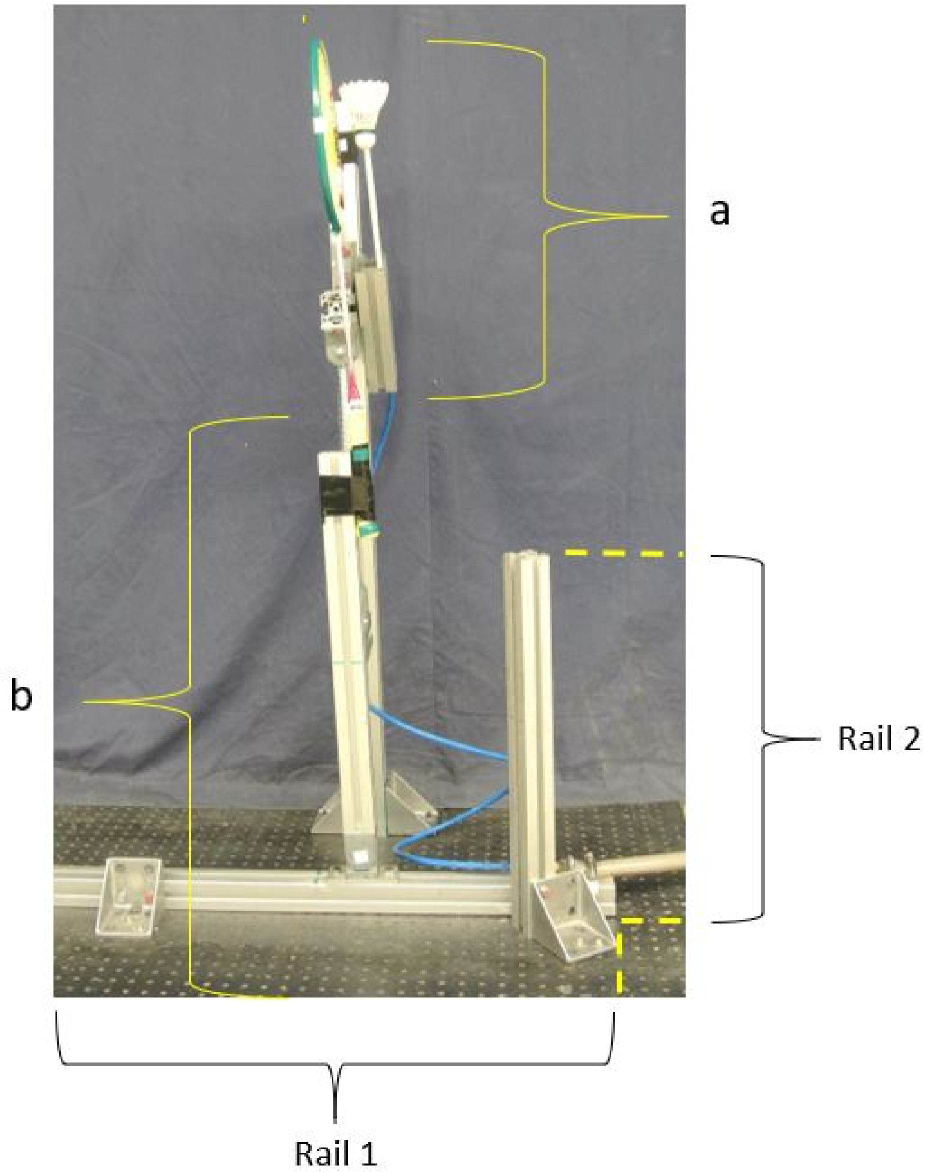

Figure 1.10: Side and front views of the experimental set up for replicating smash using spring loaded mechanism (SSLM).

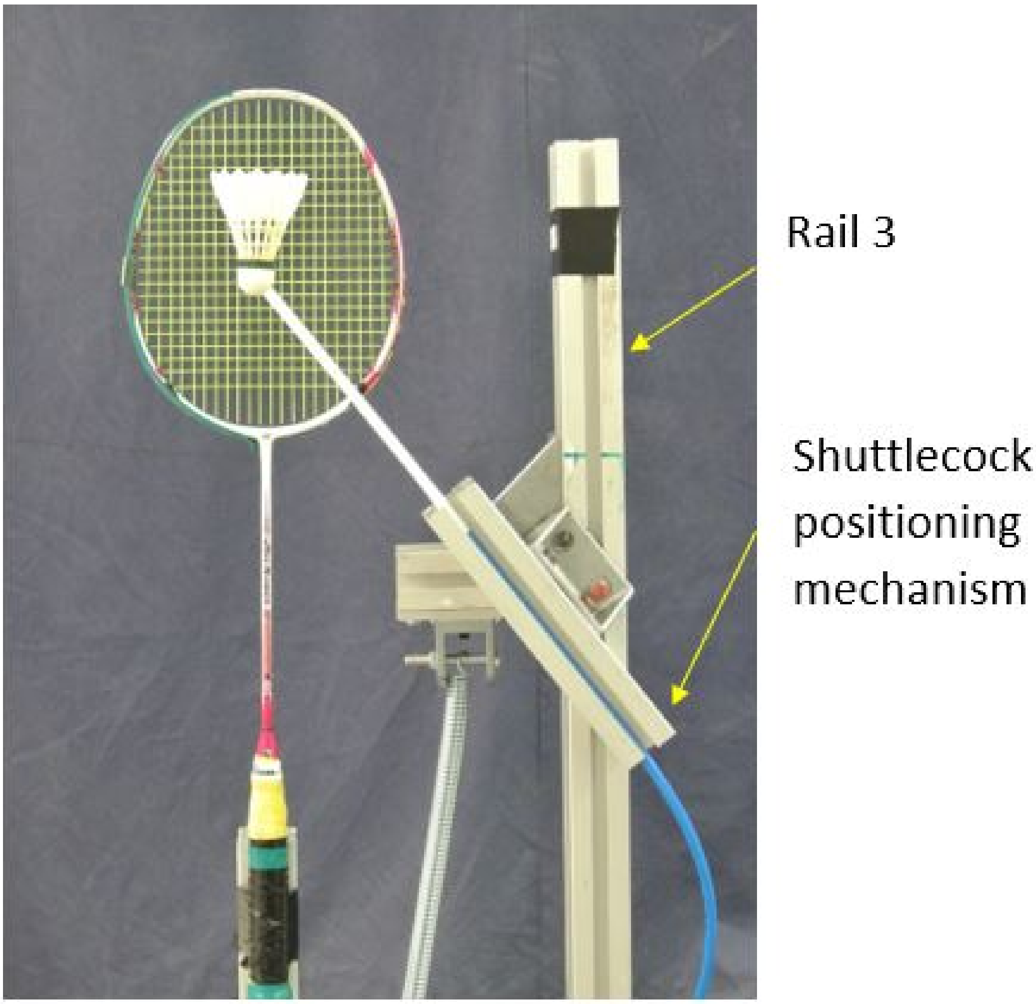

Figure 1.11: Front view of upper portion or portion '**a**' of SSLM.

2
Aim

The aim of this phase of the project is to further develop the smash and tumble mechanisms created in the previous to overcome their main limitations these involve:

- Increasing the smash speed from 25 m/s to 40 m/s.
- Increase the repeatability of the tumbling process by as much as possible.
- To produce realistic amounts of tumble for each brand tested.
- To create significant difference in tumbles between the tested brand.

3

Development Work

3.1 Smash Rig Improvements

3.1.1 Previous Test Rig and Limitations

The mechanism finalized in the previous phase had the advantage that the racket always struck the shuttlecock with the same speed and at the same position ensuring repeatability of the test. The mechanism also undergoes damping motion after the smash where it oscillates back and forth before coming to rest, this ensured that the racket does not undergo sudden deceleration and gets damaged from the mechanical shocks associated with it.

However, the mechanism had the drawback that it could only produce speeds below the required speed of 40 m/s. In normal conditions the setup could produce a speed of 15 m/s consistently and by overstretching of the spring a maximum racket tip speed of 25 m/s was achievable however this speed was not sustainable as the overstretching of the springs from repeated testing was found to permanently damage the springs. Thus the aim of the current phase was to sustainably achieve required speeds

3.1.2 Improvements - Trial and error

The initial approach towards achieving the required smash speed was following a trial-and-error method where a small modification would be made to the rig and based on the outcome, the modification was kept, refined or new modifications were added.

The design from the previous iteration consisted of only one spring attached to one side of the rotary arm, as the first step towards improvement another spring was attached to the opposite side of the rotary arm. Since more force was now generated from the same stretching of the rotary arm the speed could be increased from 15m/s to 20 m/s without overstretching of the spring, also the previous design had inaccuracies in striking the shuttle at the centre of the racket (which was the preferred position) as the stretched string exerted sideways forces in only one direction which caused the racket to tilt sideways while undergoing smash, but with the addition of an equal force spring on the opposite side this deviation was significantly reduced.

The rotary arm undergoing partial rotation had rotational kinetic energy and since more mass would require more energy to move fast, the next step was to reduce the mass of the rotary arm, thus the arm was replaced by a miniature version of the flex link member (from a 44mm x 44mm member to a 22mm x 22mm member) as shown in the fig 3.1. This helped increase the nominal racket tip speed to 26 m/s.

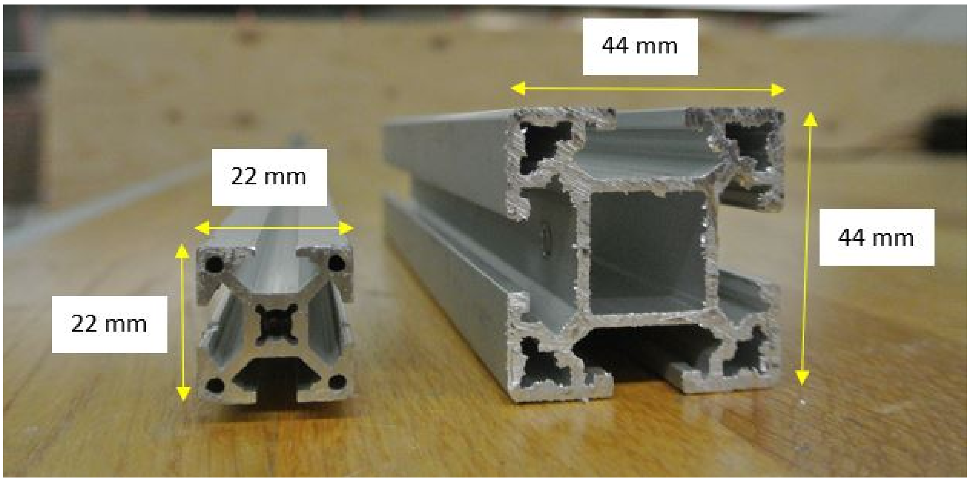

Figure 3.1: flex link used in the previous iteration on the right and flex link used in the previous iteration on the left.

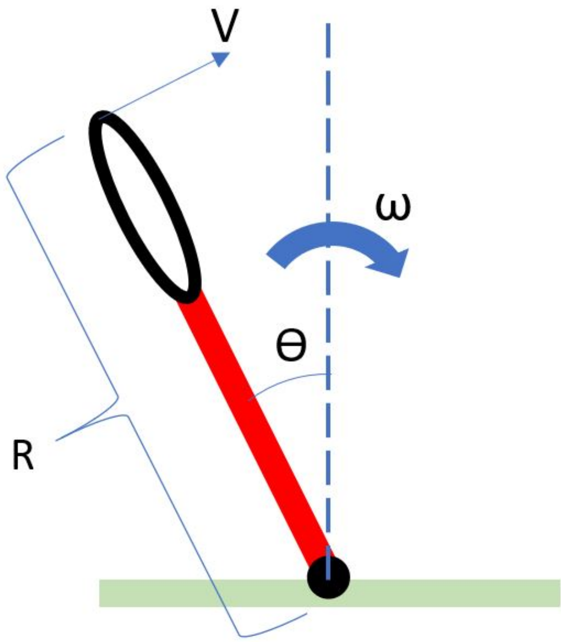

Figure 3.2: Illustration of rotary arm undergoing rotational motion with highlighted parameters.

A body undergoing rotational motion (refer figure 3.2) will have an angular velocity 'ω', that is it will cover a specific angle within a given time, for such a body (which in this case is the rotary arm and the racket) , If you increase the length of the arm 'R' the tip speed 'v' will increase, understanding the principles it was decided to extend the length of the flex link from 1m to 2m in order to increase the speed of smash. In theory this should double the smash speed, however extending the flex link also doubled the mass of the rotary arm, furthermore a faster swinging arm create more friction at the hinge. The combined effect of all these factors was that the smash speed only increased from 26 m/s to 30 m/s.

Since the racket was now travelling significantly faster it started to experience high inertial forces. The racket was connected to the rotary arm in such a way that the handle portion of the racket was attached firmly to the flex link member of the rotary arm while the shaft and head portion of the rackets were hanging freely, because of this now when the flex link underwent rotational acceleration the handle potions moved instantly with the flex link while the shaft and head potions experiences a delay in motion due to the high inertia (refer figure 3.4), subsequently the head and the shaft would spring back and overshoot the handle (refer figure 3.5) which would in turn bend the head and shaft potion in the opposite direction (refer figure 3.6) and this in turn caused them to spring bring back again (refer figure 3.7). This back and forth swinging of the head and shaft would continue throughout the motion of the rotary arm and as a consequence of this the head which used to hit the shuttlecock straight was now hitting at the random angles sending the shuttle flying in random directions. Initial attempts were made to adjust the speed of the rotary arm so that the rate of oscillation would change and the rackets would attain a straight head in between its oscillation at the point of impact . However this proved to be very tricky, a simpler solution was to increase the length of the rotary arm and attached the head shaft and handle firmly to this member making the racket behave as a rigid body eliminating wobbling. Even though this increased the mass by a fractional amount it was very effective in controlling the wobbling (as can be seen from figures 3.8 to 3.11)and making the mechanism repeatable.

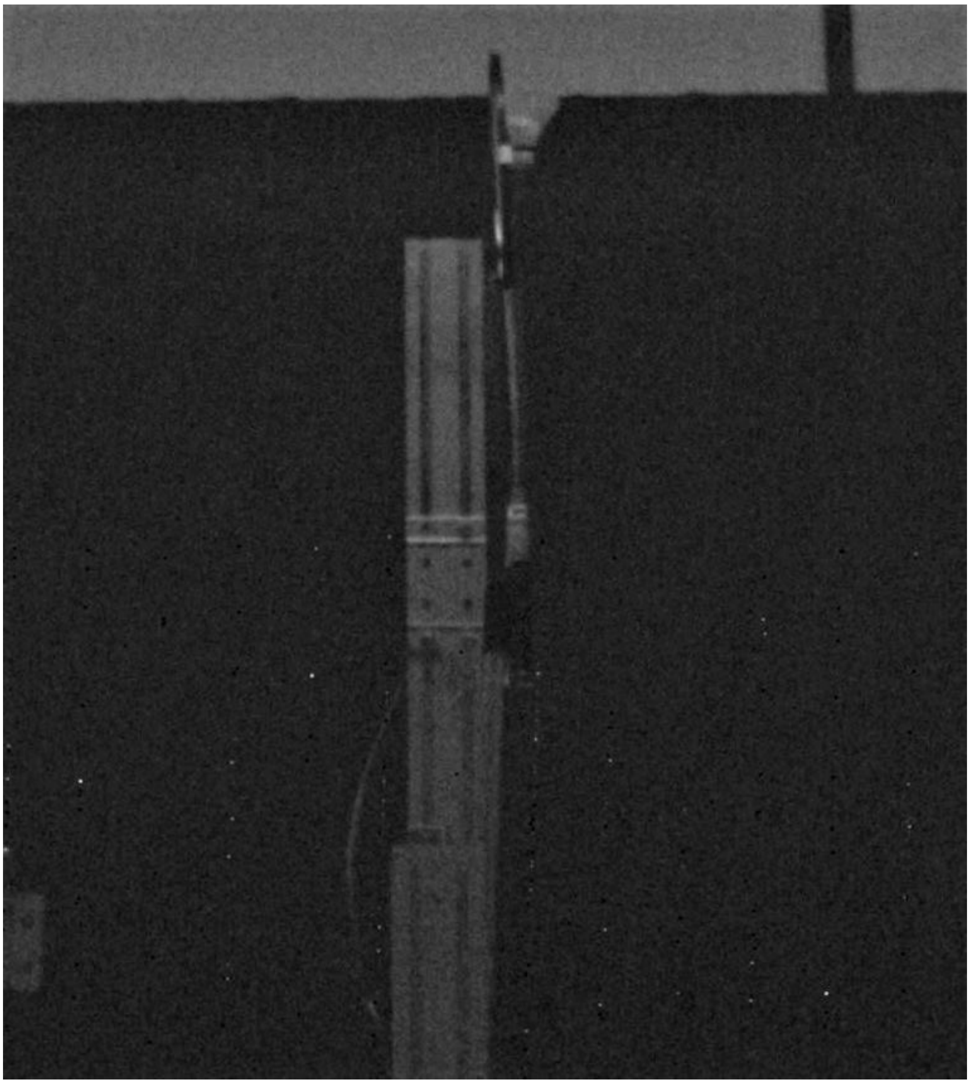

Figure 3.3: Smash occuring at oblique angle.

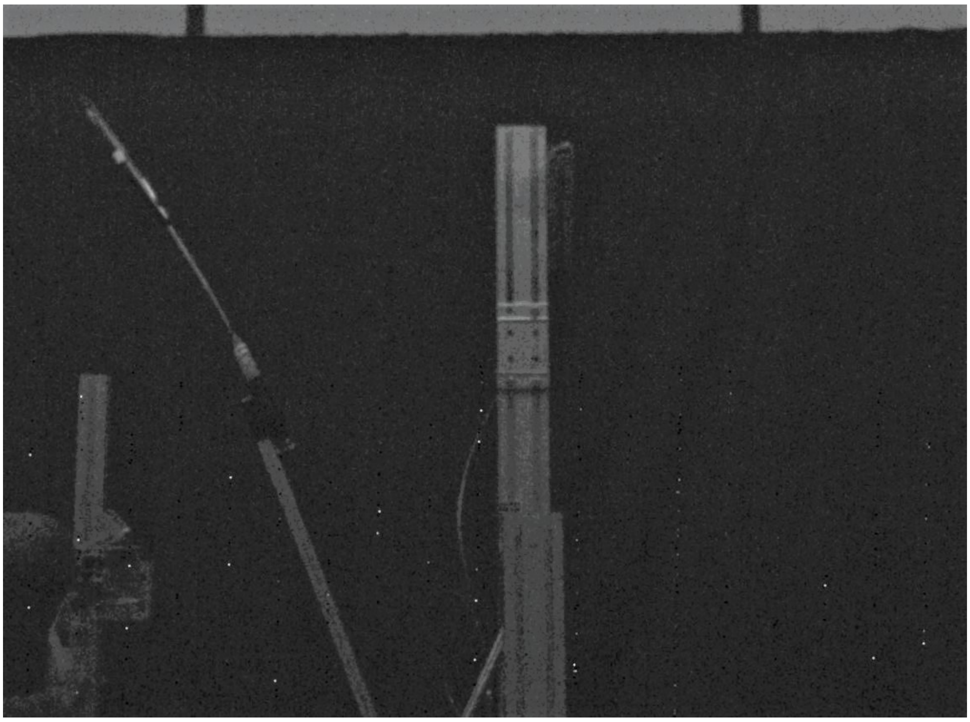

Figure 3.4: Head and shaft of the racket flexing back due to inertia before smash.

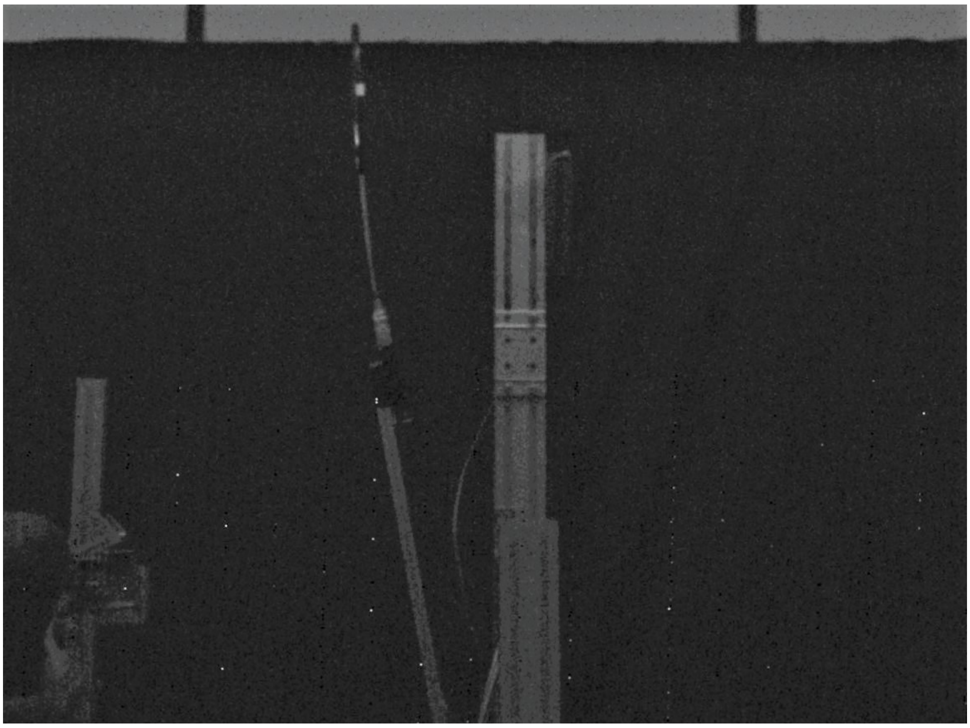

Figure 3.5: Head and shaft of the racket overshooting the handle due to the spring back effect before smash.

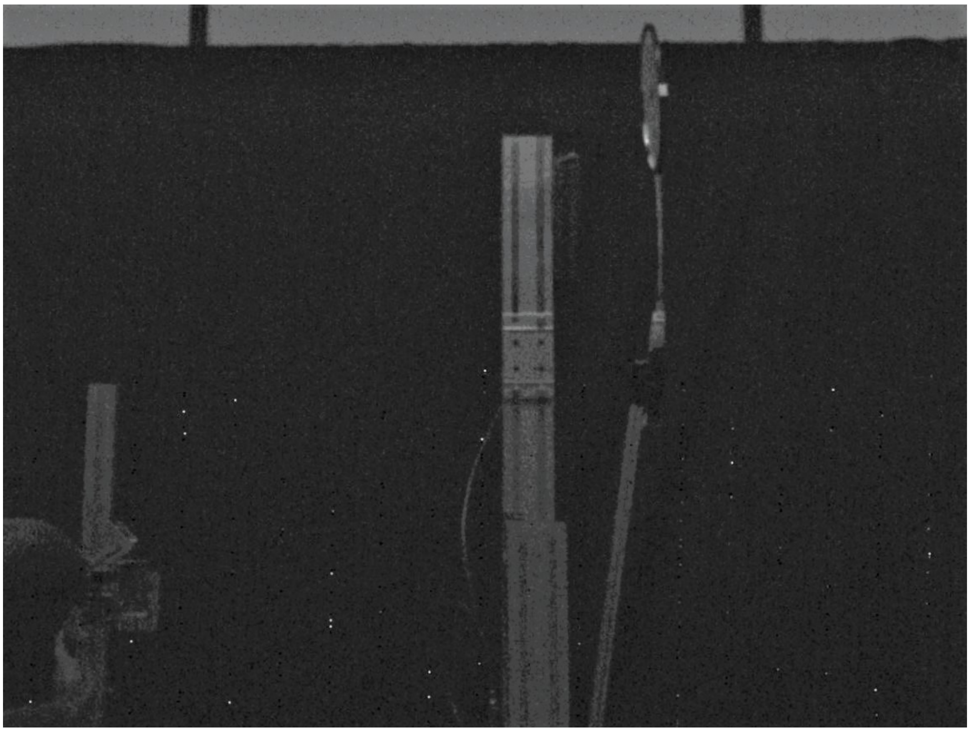

Figure 3.6: Racket flexing back during smash

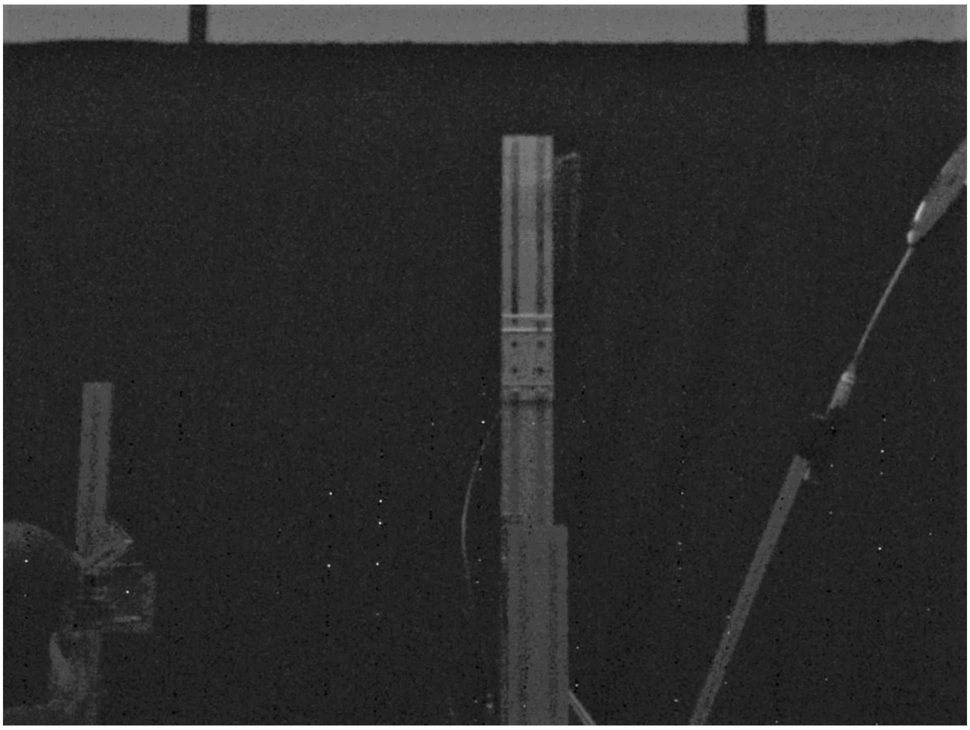

Figure 3.7: Racket springing forward after smash

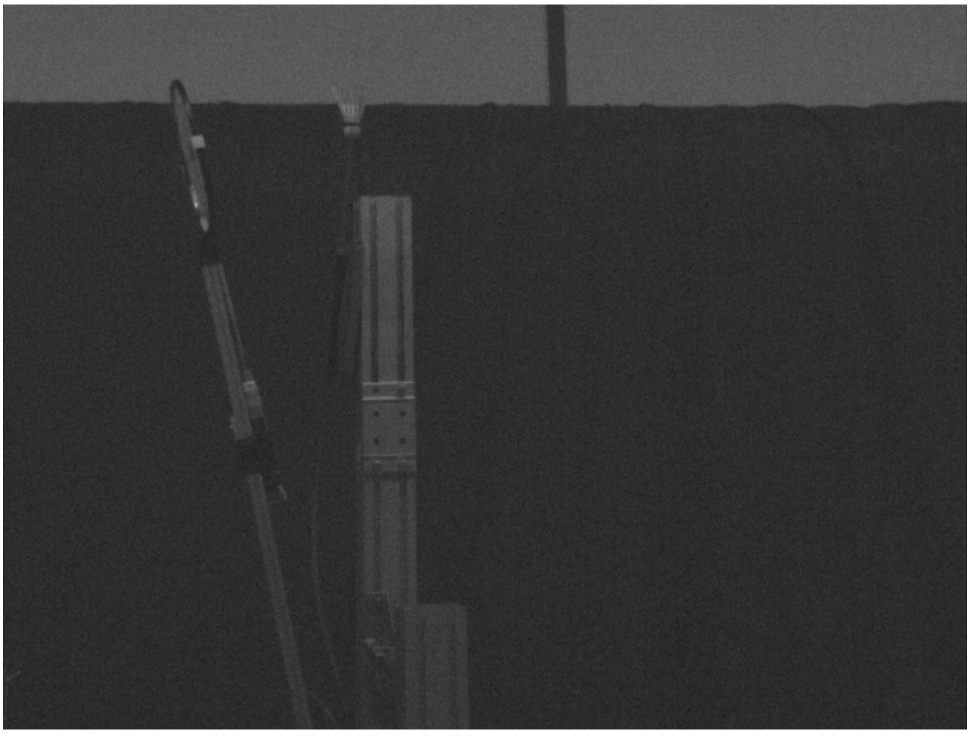

Figure 3.8: Proper Smash motion after fixing the wobble, instance 1.

Figure 3.9: Proper Smash motion after fixing the wobble, instance 2.

Figure 3.10: Proper Smash motion after fixing the wobble, instance 3.

Figure 3.11: Proper Smash after fixing the wobble, instance 4.

In an attempt to increase the speed further springs with higher stiffness were tested, this approach was based on the assumption that a spring with higher stiffness generates a higher force for the same amount of extension which is evident from the spring equation $F = K\Delta X$ [1] (Also refer figure 3.13). Two pairs of different springs of stiffness higher than the current version were tried, however it was found that they produced lower speeds than the softer spring. This was because as the stiffness increases more force is required to extend the spring which would store more energy in the spring and when released would result in a higher speed of smash, however springs of higher stiffness were also found to have a significantly less allowable range of extension, and without enough extension of the spring enough energy would not be stored in the spring which would results in lesser smash speed. The combined result of these two opposing effects were that stiffer springs produced lesser speeds than softer springs, thus this attempt was not fruitful.

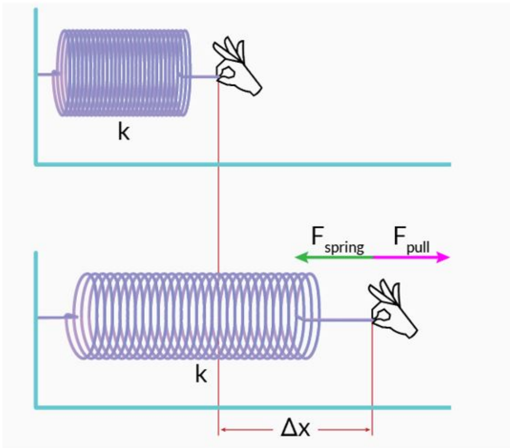

$$F_{Spring} = -K\Delta X$$

Figure 3.12: Spring equation with illustrated factors [2]

Figure 3.13: Higher stiffness springs tested: on the left, spring of K= 13.5 N/mm and on the right, spring of K= 6 N/mm

After several smash tests it was observed that the rotary arm experienced buckling, as it was now very long, very thin and experiencing high forces repeatedly. To solve this a thicker flexing member (such as a 44mm X 44mm flex link) should be used, however adding thickness to the member also increases the mass (in this case by four times). The best solution was to replace the current member 22mm x 22mm with a 44mm x 22mm member (refer figure3.15), this would make the rotary arm thicker in the direction of the force reducing buckling while mass only increases relatively minimally (in this case by only twice). This modification was successful in preventing buckling however the smash speed dropped to 23 m/s.

Since the flex link modification reduced the smash speed, in order to compensate it was decided to minimize the mass as much as possible while having a long rotary arm, as changes in these two directions proved to be fruitful from the previous iterations. Two carbon fiber hollow shafts were are used to to replace the flex link members of the rotary arm. The bottom carbon fiber member about 1 m long, where the spring and the hinge were connected was chosen to be of larger diameter and higher stiffness (and hence higher mass) as this part experienced higher loads. A shaft of smaller diameter, lesser stiffness and lesser mass was connected to the base shaft in order to extend the length of the rotary arm to 2 m measuring till the racket tip. This modification reduce did the mass of the system significantly and helped in achieving speed of about 30 m/s

After this point it seemed like most of the major fixes were done to the mechanism, modifications based on trial and error did not seem to generate significant improvement anymore, thus it was decided to change the methodology and look into the complete physics of the system in order to have a deeper understanding of the system.

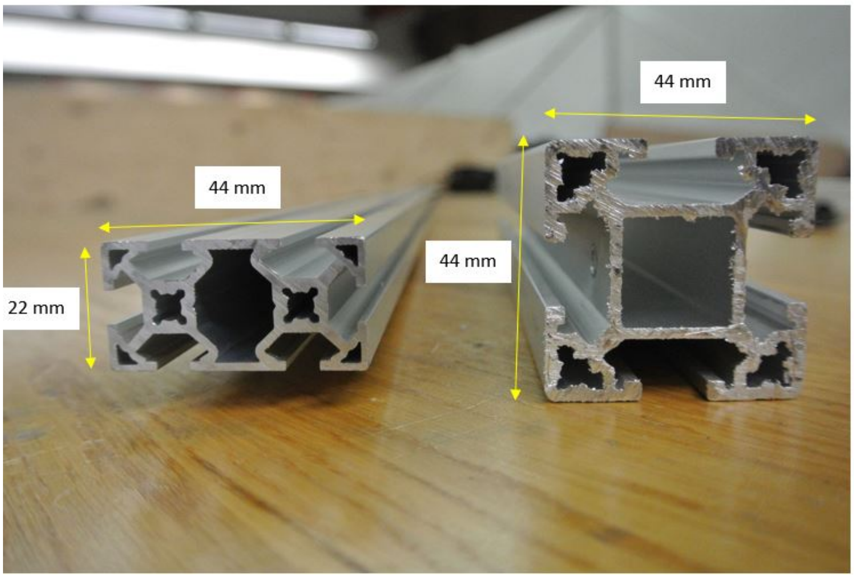

Figure 3.14: 44mm X 44mm flex link member on the right and 44mm X 22mm flex link member on the left

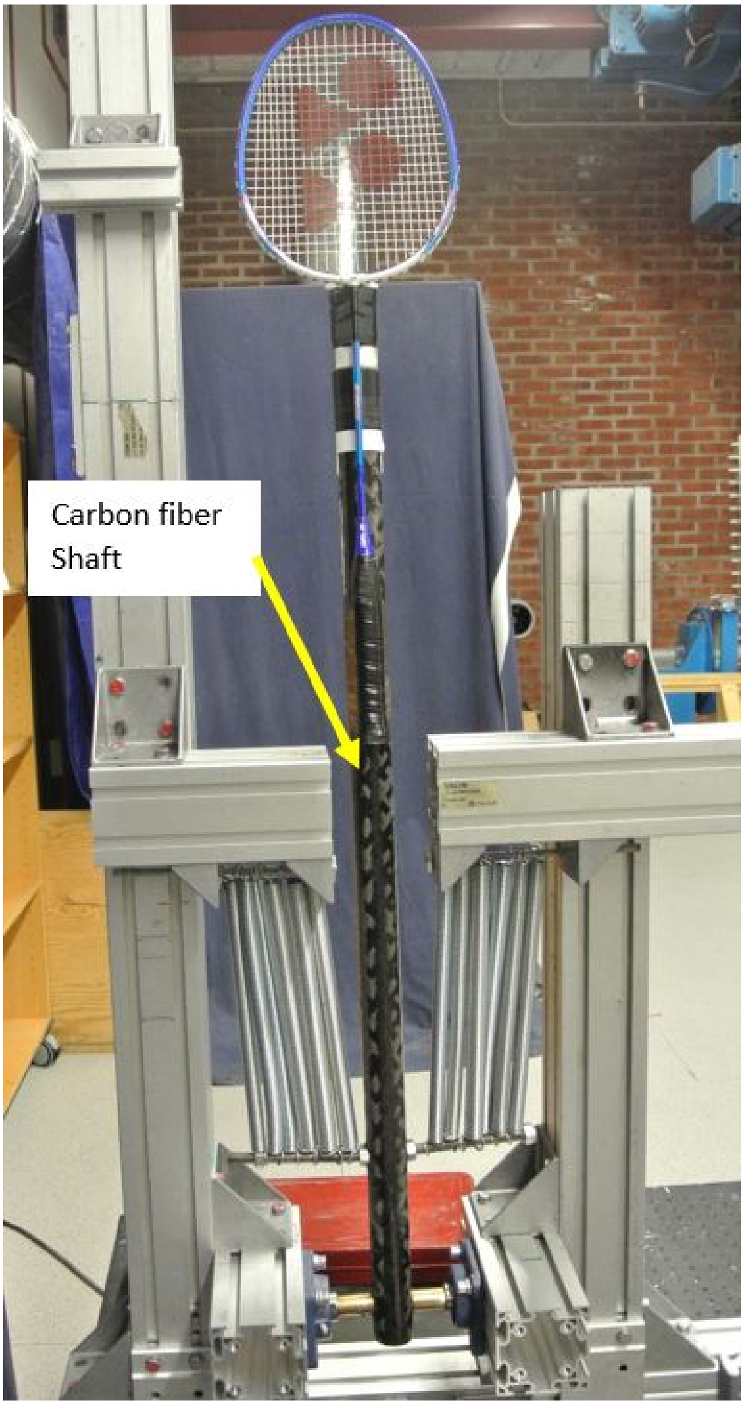

Figure 3.15: Carbon fiber shaft rotary arm

3.1.3 Improvements - Theoretical approach

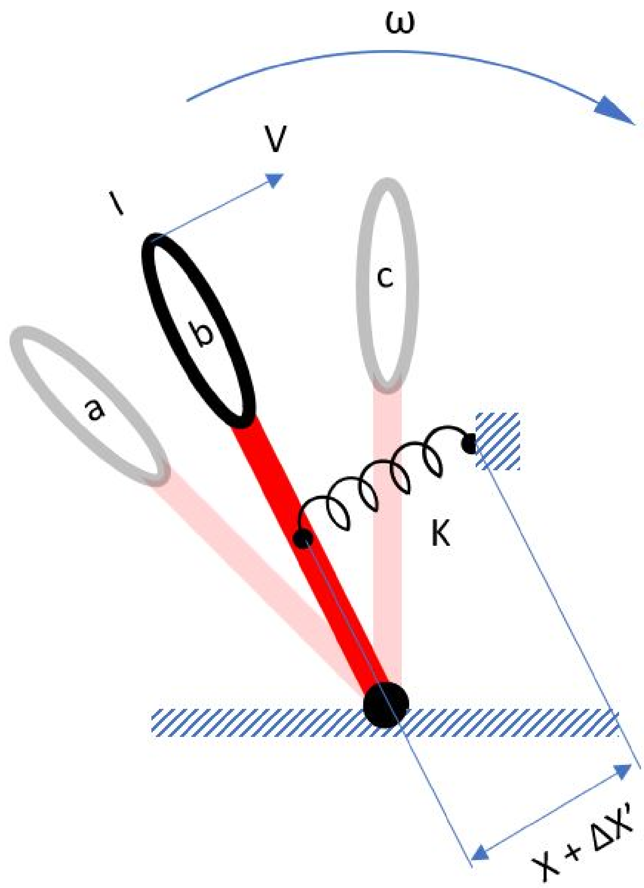

Figure 3.16: Schematic diagram of the experimental set up for replicating smash using spring loaded mechanism.

A simplified version of the mechanism is represented in the figure 3.16, it consists of a rotary arm hinged to the ground while the other end consist of the racket and a spring whose one end is fixed in space while the other end is connected to the rotary arm. To load the mechanism the rotary arm is pulled back to position 'a' and held there, at this state the mechanism does not have any kinetic energy as no parts are moving, but the spring is being stretched to the maximum (from X to X+ΔX)and hence it has maximum potential energy at this position. The potential energy stored in the spring is given by the equation [**?**]:

$$E_{Potential} = \frac{1}{2}K(\Delta X^2) \tag{3.1}$$

When released from position 'a' the spring begins to contract and so its potential energy reduces, this energy lost by the spring gets converted into the rotational kinetic energy of the rotary arm (assuming there are no other losses such as friction) and hence rotary arm gains more speed, at all positions in between 'a' and 'b', the system has non zero of rotational kinetic energy and spring potential energy

When the rotary arm reaches position 'b', the spring has contracted to its original length and hence has given up all its potential energy, Thus the system only has rotational kinetic energy at this position given by the equation[3]:

$$E_{Rotational} = \frac{1}{2} I \omega^2 \tag{3.2}$$

Since energy is conserved, the total energy we put into the system must be equal to the total energy of the system at any given time assuming there are no losses. In other terms the total energy at position 'a' must be equal to the total energy at position 'b', giving us the relation:

$$\frac{1}{2} K(\Delta X^2) = \frac{1}{2} I \omega^2 \tag{3.3}$$

Simplifying this equation we get the relationship for angular velocity of the rotary arm as:

$$\omega = \Delta X \sqrt{\frac{K}{I}} \tag{3.4}$$

Using the relationship for linear velocity and angular velocity we can derive the racket tip speed as:

$$V = R\omega \tag{3.5}$$

Thus,

$$V = R(\Delta X) \sqrt{\frac{K}{I}} \tag{3.6}$$

Assuming the rotary arm to be a solid cylinder spinning at its end (even though the rotary arm is a hollow cylinder,the moment of inertia is very similar to a solid cylinder and has been checked analytically), its moment of inertia is given by [4]:

$$I = \frac{1}{3} M R^2 \tag{3.7}$$

Substituting 3.7 in 3.8, we get the final equation of the racket tip speed as:

$$V = \Delta X \sqrt{\frac{3K}{M}} \tag{3.8}$$

A few observations can be made from this equation,ΔX And K are the two properties of the spring, of which ΔX is shown to have a higher influence on the smash speed compared to K, thus from the equation a soft spring that can extend more would create a higher smash speed compared to a stiff spring that can extend less, which has been observed from previous experiments. It can also be deduced from the equation that adding more springs would be effective, as in doing so the parameter 'K' gets multiplied by the number of springs while the parameter 'ΔX' remains the same, thus multiplying the velocity by a factor of $\sqrt{K}$. Furthermore from the equations reducing the mass increases the smash speed but not significantly (only by square root) which has also been observed from previous experiments. Another important observation was that the length of the rotary arm has no influence on the smash speed, this is contradictory to the previous experimental observations in which an increase in the rotary arm length had a positive influence on the smash speed, in order to understand why this happened we must also look into the physics of loading the mechanism.

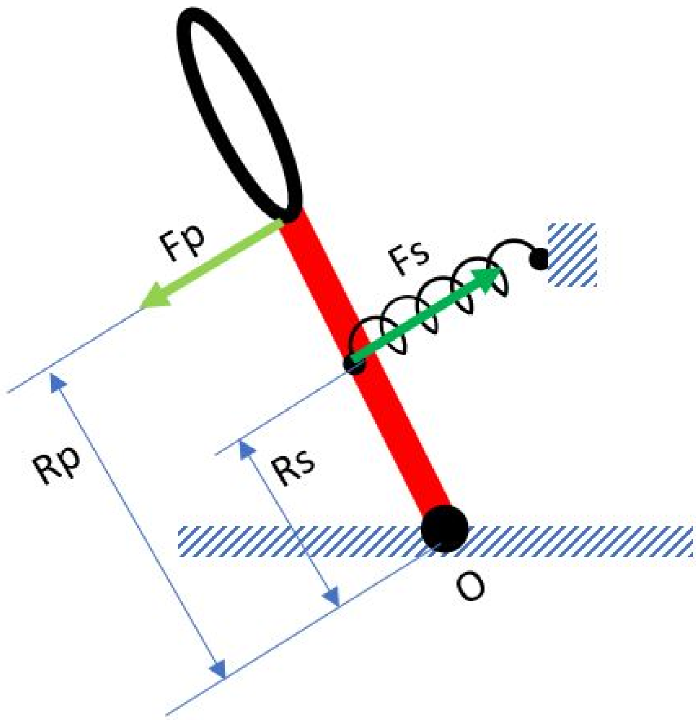

Figure 3.17: Schematic diagram of loading mechanism of the rotary arm with depicted parameters.

As shown in the figure3.19, 'o' is the hinge of the rotary arm, the spring is attached at a distance 'Rs' from 'o', when the arm is stretched back the spring produces a force 'Fs' which creates a moment across o (here, in the clockwise direction). To at least hold a rotary arm in this position an equal moment must be applied in the opposite direction, this is done by giving a pulling force 'Fp' to the rotary arm at a point 'Rp' distance from 'O', equating the two moments produced we get:

$$F_p R_p = F_s R_s \tag{3.9}$$

rearranging the equation we get the minimum loading force requires as,

$$F_p = F_s(\frac{R_s}{R_p}) \tag{3.10}$$

It can be seen from the equation that as 'Rp' increases the pulling force required 'Fp' to load the mechanism decreases, this is the basis of the anomaly observed in the previous experiments. Since the rotary arm was longer, it required less force to stretch the spring, however nearly same amount of force was being applied to both long and short rotary arms, which resulted in the case of longer arm to stretch the springs more, which ultimately lead to a higher smash speeds.

The understandings from equation 3.8 led to the following modifications: The carbon fiber extension was discarded and only the base carbon fiber shaft was used in order to reduce mass, soft springs were used and their number was increased from 2 to 6 as calculations showed that this would be sufficient for achieving the required smashed speed.

However these modifications could only bring the speed up to about 32 m/s, which seemed to deviate largely from the theoretical predictions, Initially it was thought that this difference in speed could be caused by frictional losses or addition of spring mass to the system which even though small was unaccounted for in the equation. To compensate for these losses it was decided to add more springs which should add more energy to the system. The springs were added sequentially and tested, it was observed that these additions still did not create significant improvement in smash speed, as a speed of only about 35 m/s was achievable even with a total of 8 springs.

After thorough investigation of individual parts of the system it was found that springs inherently had a speed limit which limited the mechanism in achieving higher speeds. Measurements from slow motion footage showed that the soft springs used had a maximum speed of 7.5 m/s. Stiffer springs were found to have higher maximum speeds however using stiffer springs were not considered as these were shown by the equation 3.8 to slow down the mechanism, still the number of springs could be increased however using new springs would lead to tuning of multiple parameters and also all available stiffer spring options were shown to slow down the smash speed, hence this idea was rejected.

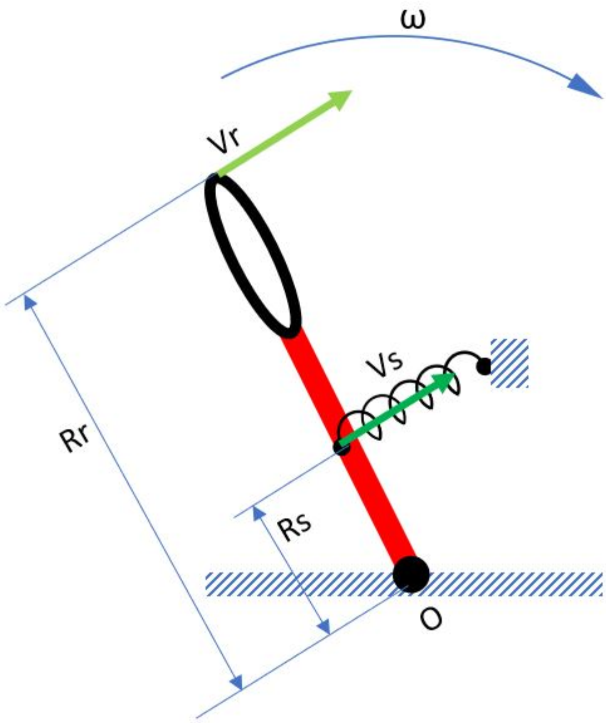

Figure 3.18: Schematic diagram showing principle of velocity with depicted parameters.

From more theoretical investigation it was found that this limitation can be compensated by adjusting the position of the spring. As depicted in the figure 3.18, when the mechanism is released the spring attachment fixed at a distance 'Rs* from the hinge will be moving with a velocity of 'Vr', this would cause the rotary arm to rotate at an angular speed of 'ω', since the rotary arm is a rigid body all points in the body must move with the same angular speed and thus the racket tip speed is given by the equation,

$$\frac{V_r}{R_r} = \omega = \frac{V_s}{R_s} \tag{3.11}$$

simplifying this equation we would get the relation of the racket tip speed as:

$$V_r = V_s(\frac{R_r}{R_s}) \tag{3.12}$$

Thus as the spring is kept closer to the hinge 'o' the racket tip speed increases,however moving the spring towards the hinge also reduces the stretching of the spring during loading. Minor calculations followed by a few trials showed that in order to achieve the required spring stretching and racket speed the spring should be attached such that the ($\frac{R_r}{R_s}$) should be about 5.3. But finally taking into account the losses in the mechanism the ratio was increased to 6. This modification was very effective and a smash speed of about 43 m/s was achieved which is slightly above the requirement.

Even though the mechanism was successful in achieving the smash speed, since the rotary arm was now significantly smaller, loading the mechanism required a very high force and was nearly impossible to be done manually. An understanding from the equation 3.13 was employed to solve this problem, a detachable steel shaft was inserted into the hole of the carbon fiber base shaft to act as a temporary extension providing leverage and reducing the required force significantly. The steel shaft would be pulled back along with the rotary arm to the required position and the arm would be locked in place with an additional locking mechanism, the rod would then be taken out followed by the release of the locking mechanism to create the smashing motion.
To create the locking mechanism, the part feeding assembly of a manually operated lathe were used. When the rotary arm is pulled back to the required position and held there, the lathe feeding mechanism fixed nearby as shown in the figure 3.19 is activated. By turning The hand wheel a feeder arm is extended to a position above the carbon fiber shaft of the rotary arm, which when detached from to steel shaft presses against the feeder arm and is held in place. Once the experimental setup is ready the hand wheel can be used to pull back the feeding arm which after reaching a certain position will not have enough contact to stop the rotary arm and hence it slips and smashes the shuttlecock.

It is to be noted that when the rotary arm slips the carbon fiber shaft tends to rub against the sharp 90-degree corner of the feeding arm which wears out the carbon fiber shaft. To prevent this a piece of plastic pipe is inserted onto the carbon fiber shaft and held in place with thick tapes, the inner diameter of the plastic pipe is slightly larger than the outer diameter of the carbon shaft thus allowing it to rotate freely without much deformation and act as a bearing. Now when the rotary arm slips instead of rubbing against the sharp corner the plastic shaft simply rolls over it protecting the carbon fiber shaft inside and allows for smoothly release of the rotary arm.

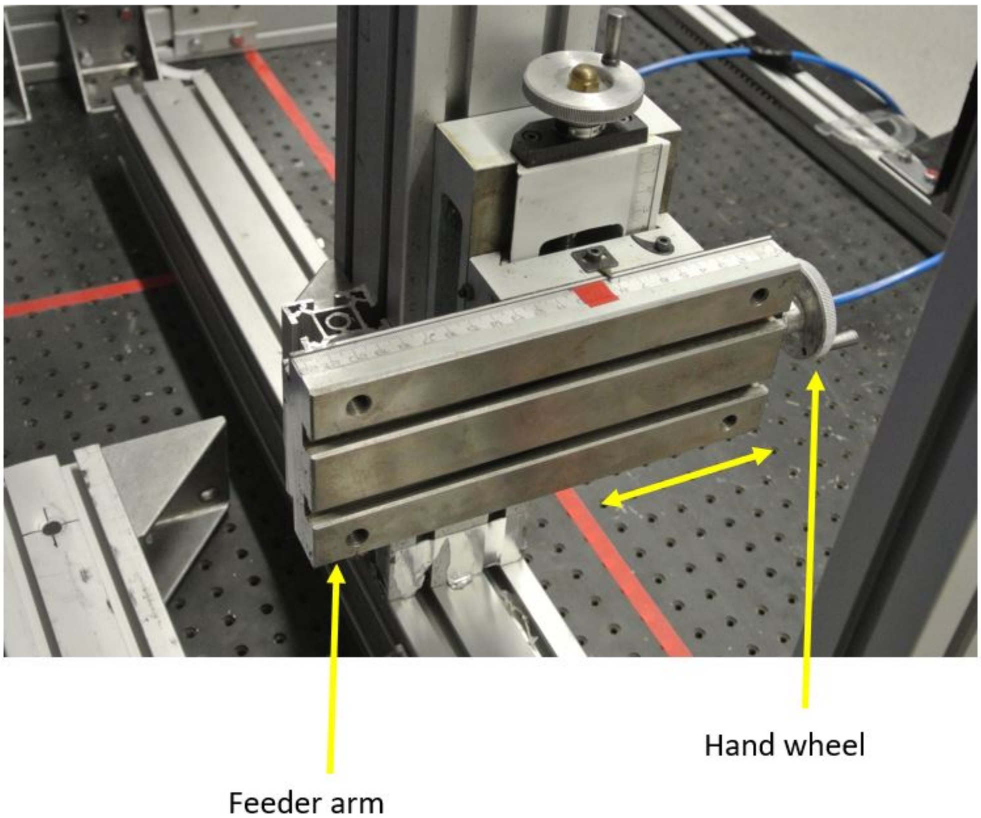

Figure 3.19: Locking mechanism.

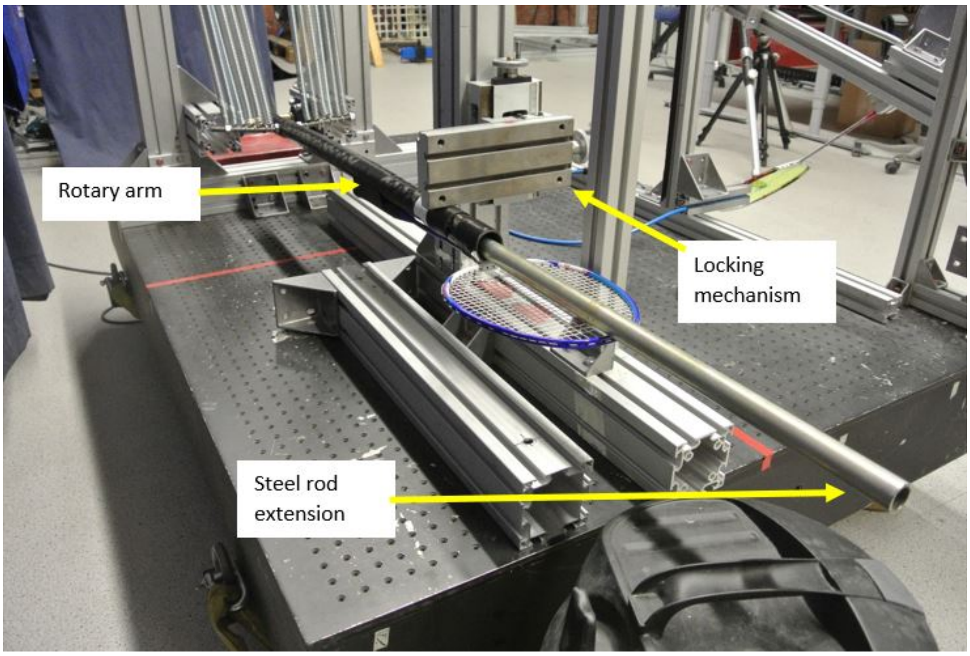

Figure 3.20: Locking mechanism isometric view.

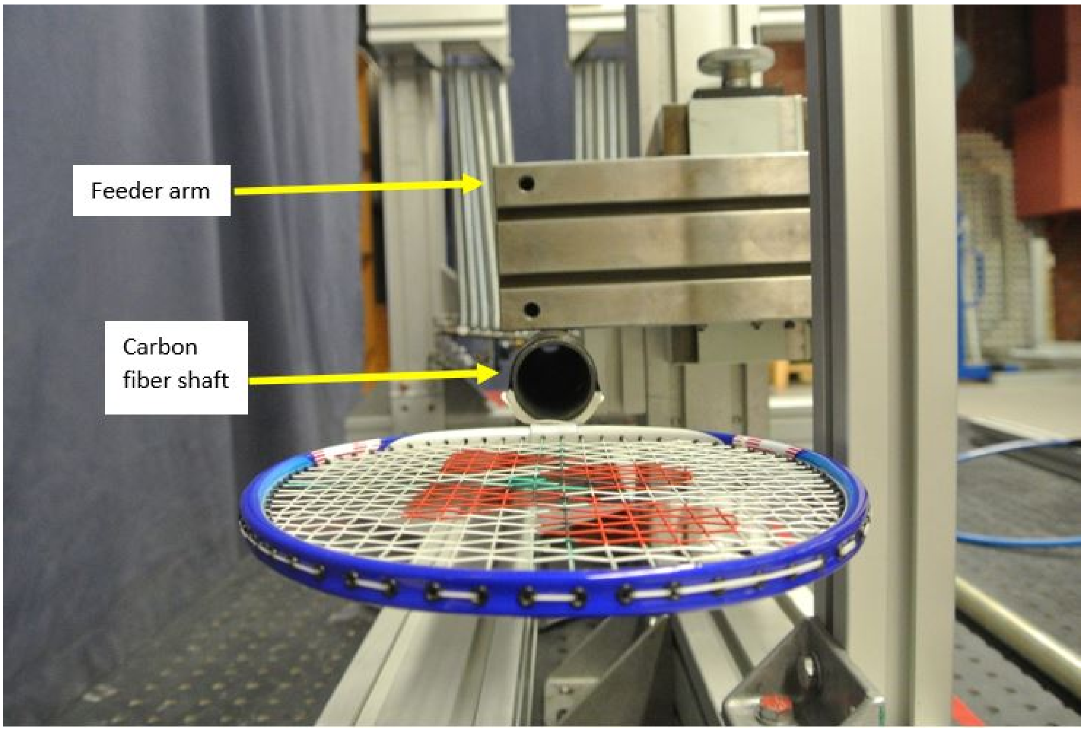

Figure 3.21: Locking mechanism front view.

Figure 3.22: Plastic bearing tube

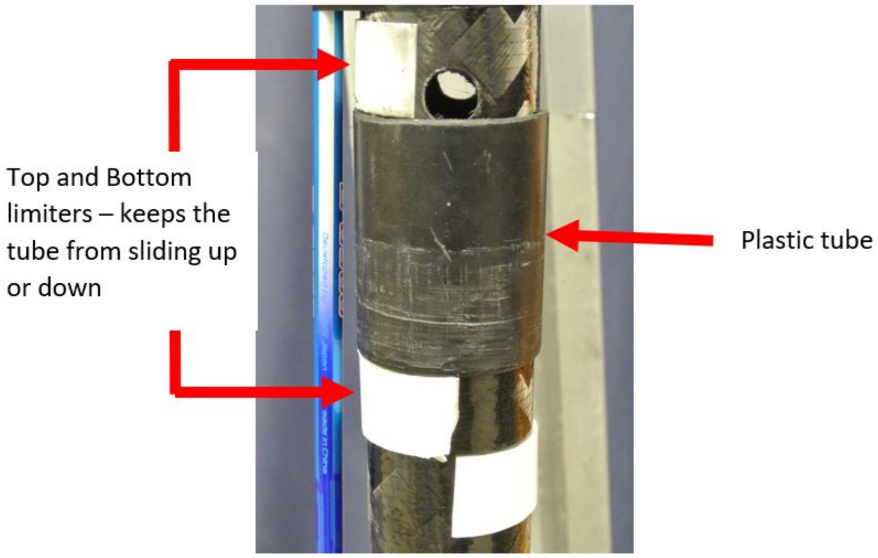

Figure 3.23: Rotary arm plastic bearing

In addition to these fixes a bearing was also added at the hinge portion in for giving less friction while preventing sideways deviation during the smashing motion of the rotary arm.

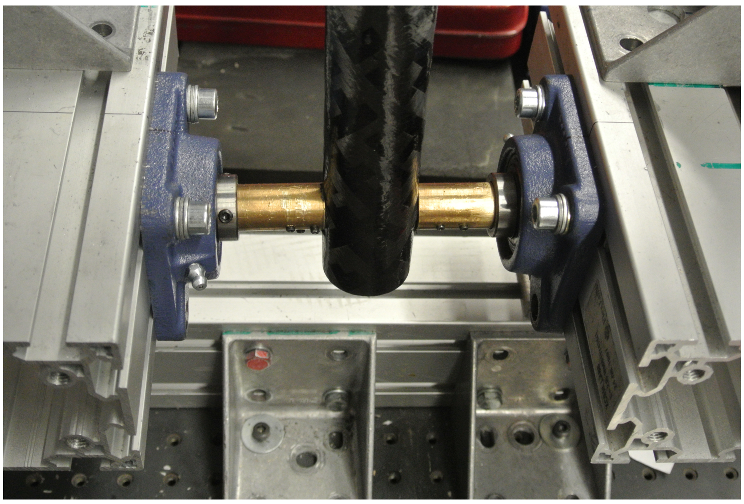

Figure 3.24: Hinge bearing

3.2 Smash test

The mechanism/test rig was found to produce required smash speeds consistently and hence the next phase of validation was to test the smash results from the rig against pre-tested shuttlecock brands.

3.2.1 experimental Setup

The experimental is setup as shown in the figure 3.27, The test rig mounted firmly on a rigid base so as reduce slips and vibrations, a cloth screen is placed about 4 m in front of the rig so as to capture the smashed shuttlecock, a camera is placed at right angles to the plane of rotation of the rotary arm and a dark screen (made of cloth) is used as background for the video.

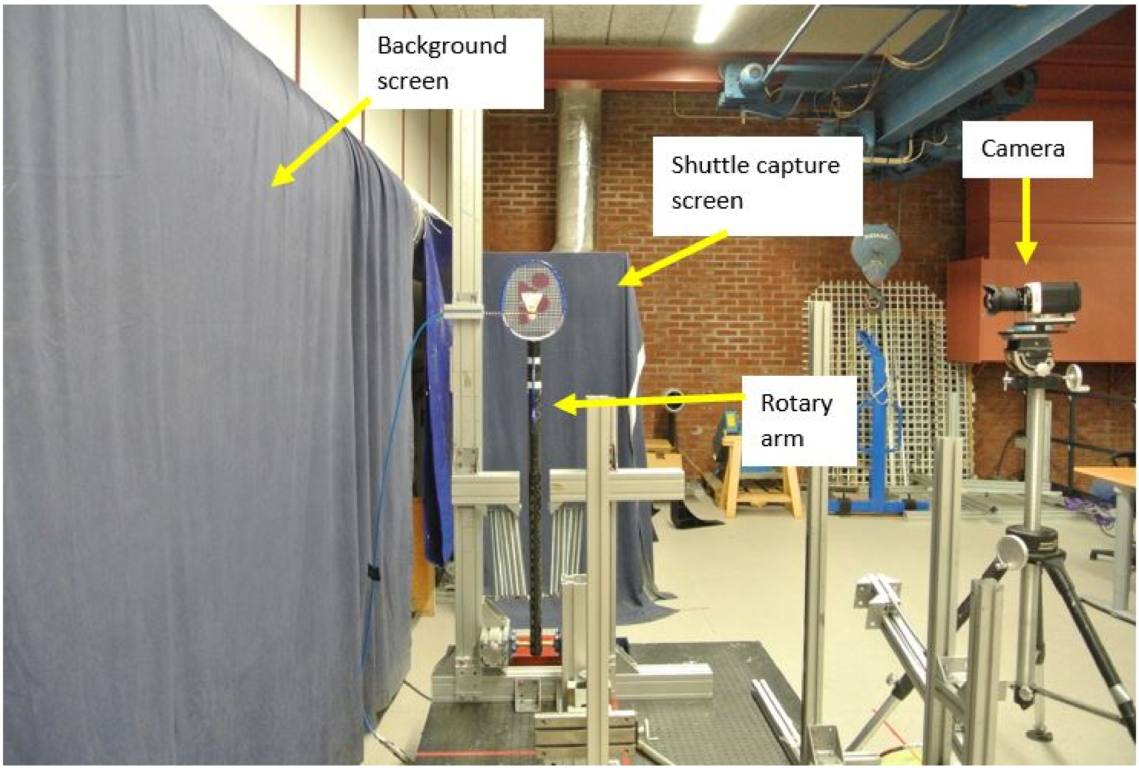

Figure 3.25: Experimental setup - back view

Figure 3.26: Experimental setup - Iso view

Figure 3.27: Cloth screen used to capture the smashed shuttle cock

Figure 3.28: Marker for velocity measurement

A marker is placed on the carbon fiber shaft at distance of 0.84 m from the hinge and the velocity of this point (denoted as 'V_m') is measured. To derive the racket tip velocity equation 3.18 is used, here the total length from hinge to racket tip is 1.22 m, hence the length ratio ($\frac{R_r}{R_m}$) is 1.452380952. The marker velocity was measured to be around 30 m/s which translates to a racket tip speed of about 43 m/s. The smash speeds for 36 tests were measured and found to be consistent, this can be seen from the table 3.43

$$V_r = V_m \tag{3.13}$$

A phantom camera was used, which is a high speed camera used usually used in research. The camera was set up to record at 8400 frames per second and at 640 x 480 pixels resolution, this was found to be the best match between video quality and recording speed required to minimize measurement errors.

Figure 3.29: The camera used for recording smash

The camera is positioned in such a way that the center of the frame is in level with the marker centre when the racket is perpendicular to the ground. this is also the position where the racket meets the shuttlecock and is termed as the contact position. The racket tip velocity at this position is taken as the reference and hence this alignment of the camera is to minimize the parallax errors at this point.

The camera is also positioned in a way as to view about 1.5 m in front from the contact point (refer figure3.30), this is done in order to view the flight trajectory of the shuttlecock.

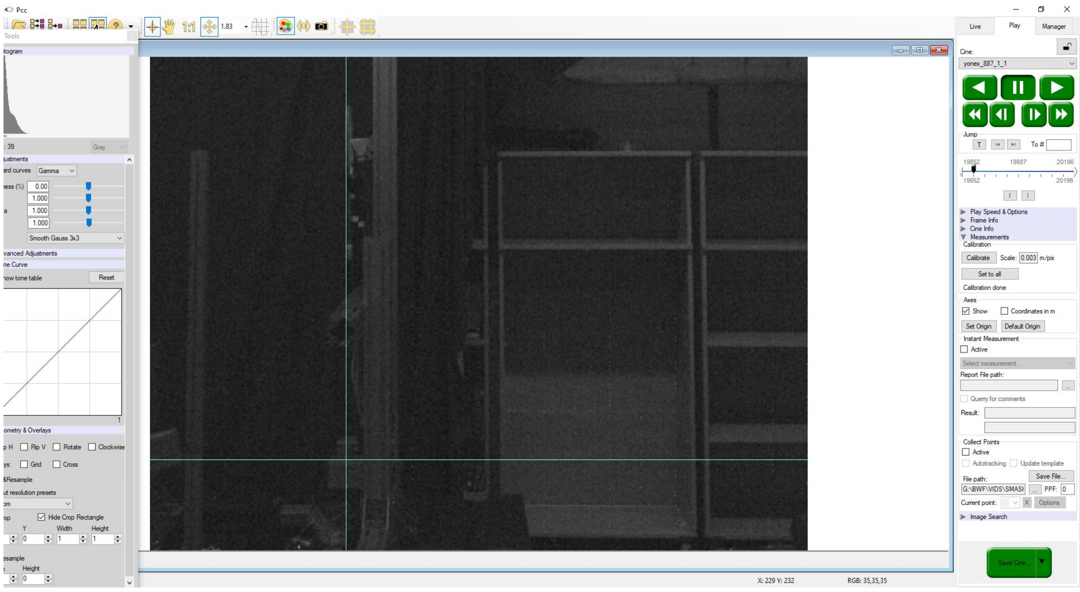

Figure 3.30: PCC interface and video frame

To post process the videos the software used was Phantom Camera Controller (PCC 3.4) which is the recommended software for phantom cameras. The interface of this software can be seen in figure3.30. during velocity measurement individual pixels of a frame can be selected for maximum accuracy hence the cross design of the marker, the pixel at center portion of the marker where the 90 degree corners of the two white squares meet at 10 frames prior to and after the contact position are selected and the average smash speed over 20 frames is calculated. However the software can be off by one pixel while selecting a pixel, in the current frame since each pixel represents 0.003 m. The measurement error in velocity was calculated to be about 2 m/s

To validate the test rig three shuttlecock brands were used all of which were of the feathered type: 887 which was the reference brand, 815 and 819 both of which were smash tested manually at RISE and were classified as not having adequate smash resistance.

3.2.2 Test Results and analysis

Three random samples from each brand were chosen and each shuttlecock had one of its feathers marked and were smashed 15 times on the marked position. During the smash the velocity of the shuttlecock was monitored. After the smash each sample was inspected for damage.

3.2.2.1 Shuttlecock Damage

The damage was identified by two means, one was by noting how much rumbling of the feathers were evident, and the other was by noting the deformation of the skirt cone from its normal circular profile.

At the end of the test it was observed that brand 887 showed the least amount of deformation / distortion from its circular profile, no deformation was observed during the first 12 smashes after which small deviations in diameter were observed, a maximum difference of about 2 mm was observed between the the squished and elongated sides. This brand also showed the most amount of rumbling on its feathers

Brand 819 produced the least amounts of rumbling on its feathers, while it produced more deformation compared to 887. No distortions were observed during the first 7 to 9 smashes after which distortion started to become more evident and a maximum distortion of about 3.5 mm was observed

Brand 815 produced similar rumbling characteristics compared to 887 but lesser, while it produced the most deformation of all the three brands. Similar to 819 no distortions were observed during the first 7 to 9 smashes after which distortion started to become more evident and a maximum distortion of about 4.5 mm was observed.

Figure 3.31: Brands 887 - side view

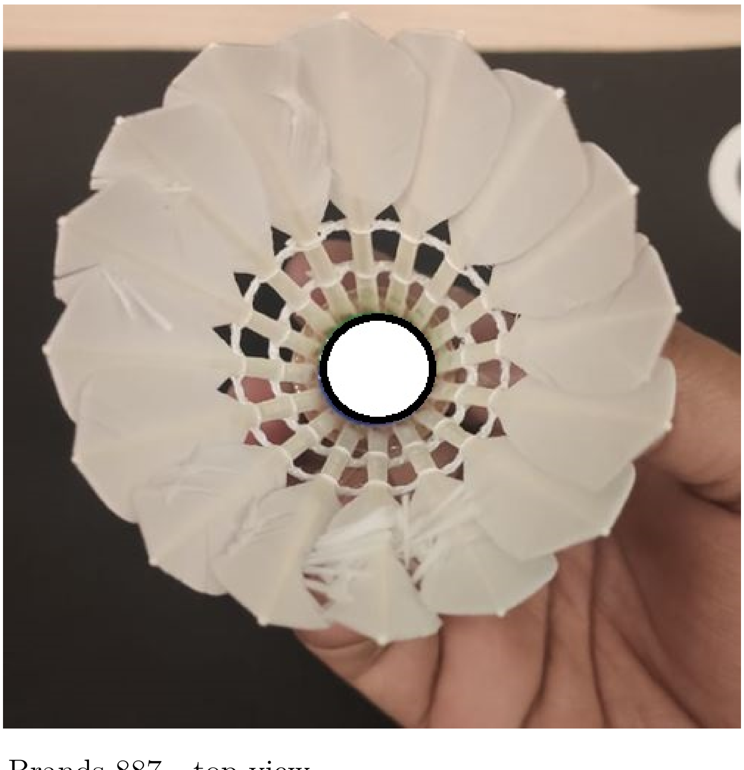

Figure 3.32: Brands 887 - top view

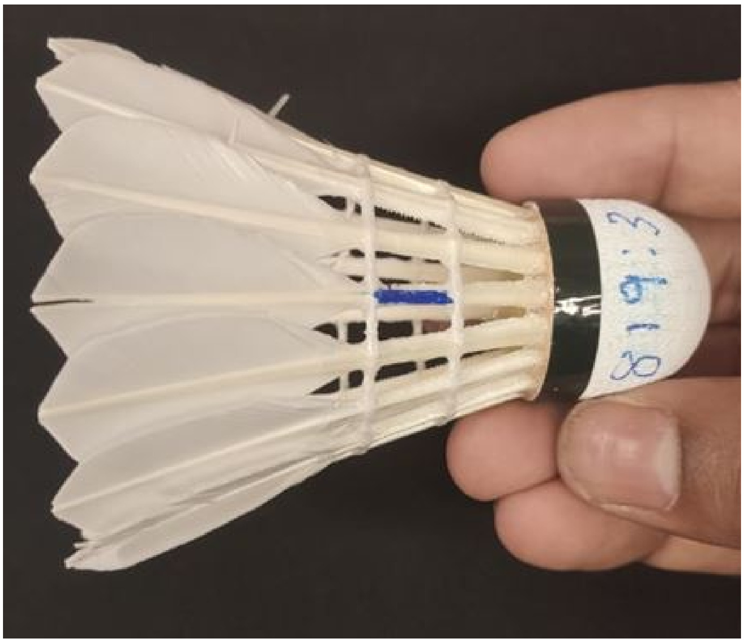

Figure 3.33: Brands 819 - side view

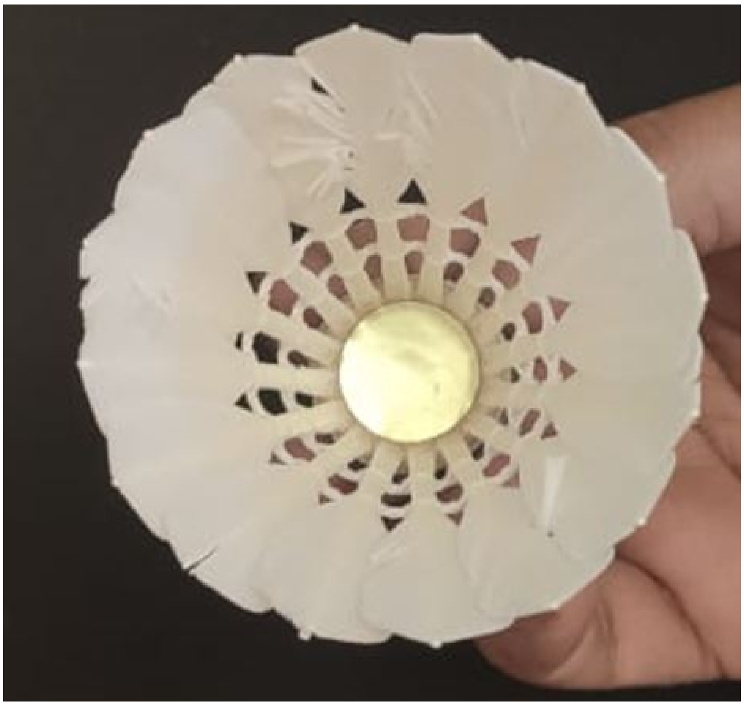

Figure 3.34: Brands 819 - top view

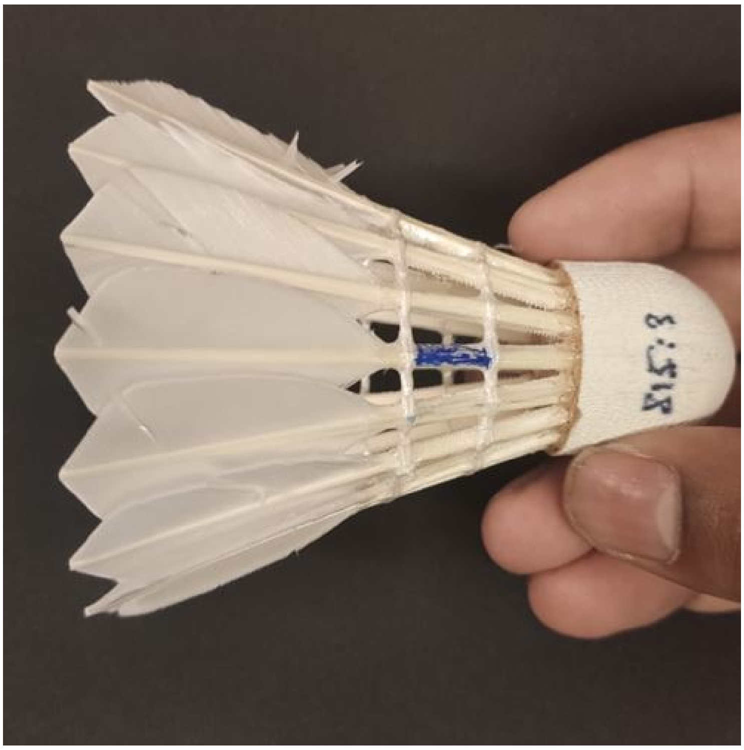

Figure 3.35: Brands 815 - side view

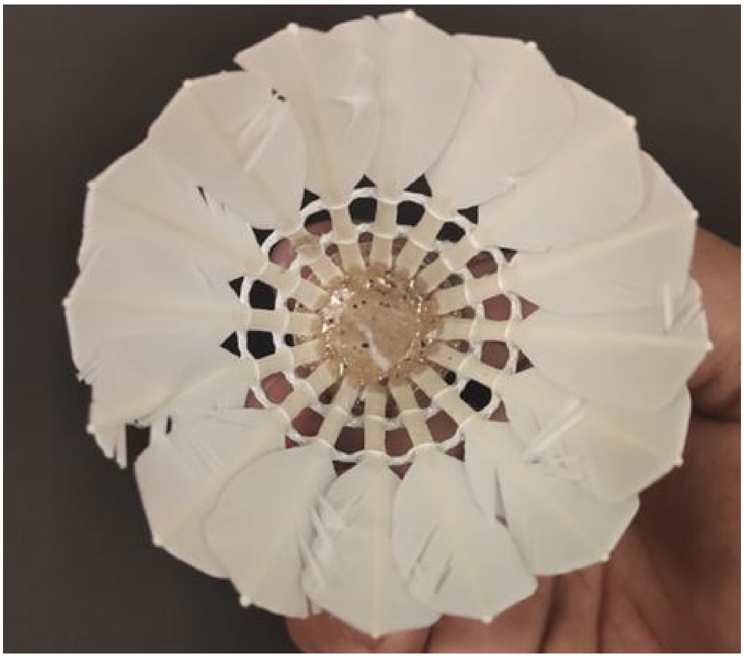

Figure 3.36: Brands 815 - top view

3.2.2.2 Skirt Compression Test

The conventional method of measuring smash resistance is through a skirt compression test in which the shuttle is placed on a flat bed and a metal disc moves down compressing it, all the while the displacement of the disc (measured in mm) and the resistance offered by the shuttle (measured in N) is monitored, the machine employed has a load measurement error of about 0.5 %. In the conventional method the given sample is smashed 10 times between two professional players and is then compression tested, the resistance offered by the shuttle at 15 mm, 25 mm and 35 mm are noted for each shuttle and these values for different samples are compared. The benchmark is a Yonex tournament shuttle which is used in professional games, a skirt stiffness lower than the benchmark is regarded as lower quality shuttlecock.

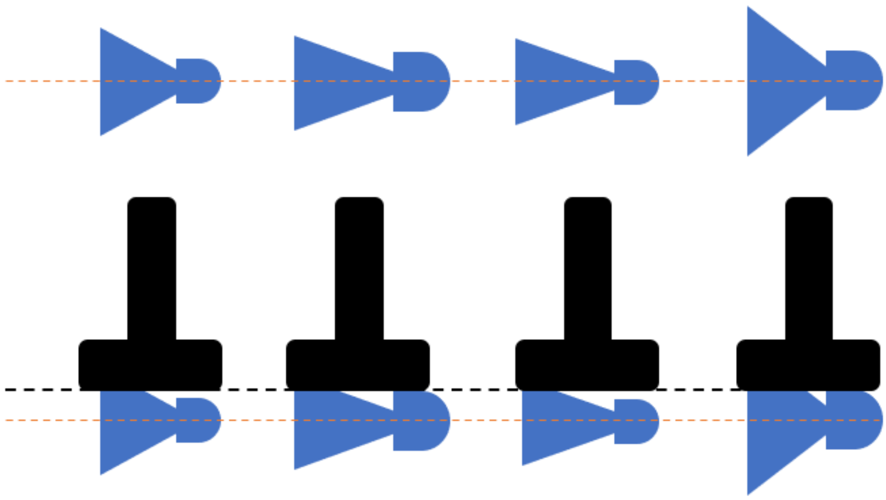

Figure 3.37: Schematic representation of compression test - Compressed to same level

This methodology had a few limitations, since different brands have different skirt cone and cork dimensions (check the figure above) if they are compressed to same displacement (marked by the black dotted line) some skirts will be fully compressed (till the cork) while some will barely be compressed. Also in a real game any shuttle irrespective of the dimensions will have its skirts compressed till the racket hits the cork. Hence if a fixed displacement is used in the compression test, in some cases we get a force from the shuttle for partial compression which may be a weak force and the shuttle may be discarded, while in the real game it would be fully compressed, would give a higher force and may be playable. Thus in order for fair testing it was initially decided that all shuttles must be compressed till the cork as shown below (note the black dotted lines). A later investigation of slow motion footage and review from Mr.Christer showed that in the real game the skirt is compressed till the diametrically opposite feathers tips touched each other, hence full compression was redefined as such. To replicate full compression displacement is only given to open end of the skirt cone until the feather tips meet.

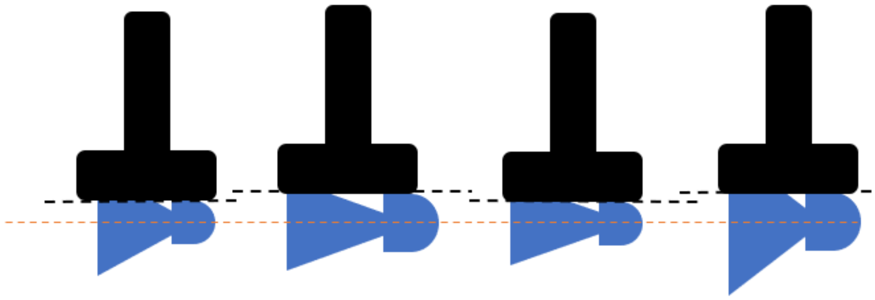

Figure 3.38: Schematic representation of compression test - Compressed to different level

The data produced from a conventional compression test of 12 brands tested at RISE is shown below.

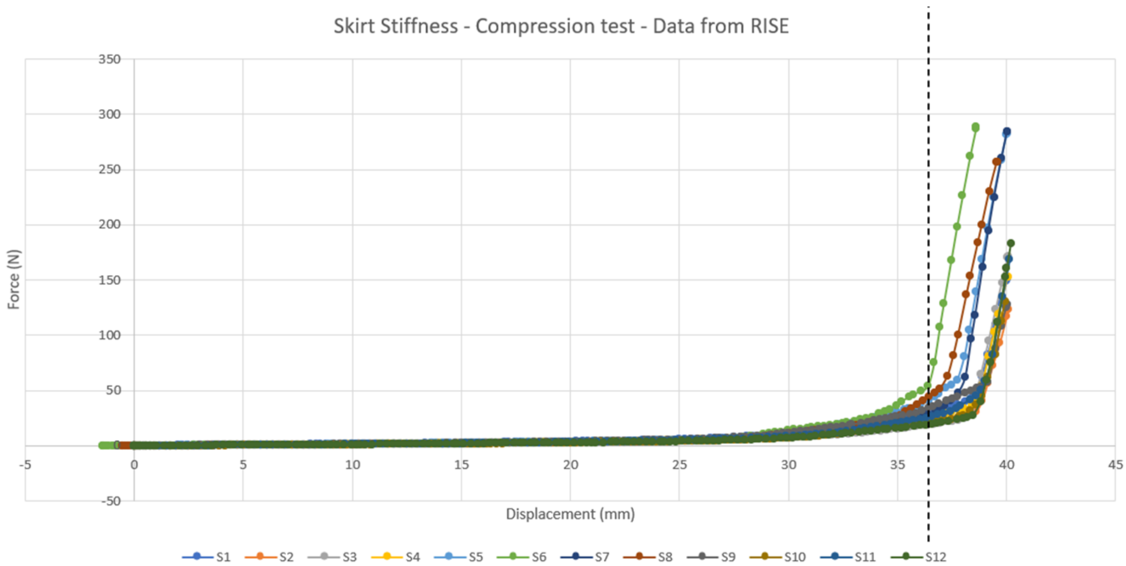

Figure 3.39: Plot of shuttle resistance versus metal disc displacement

In this graph, the conventional method of comparing performance will work for samples of one brand or between the same sample before and after the damage as they have the same geometry. However for samples of different brands this method is not valid, to understand refer figure 3.39 here check the black dotted line, at this displacement sample 6 (S6) has reached the cork or is at full compression while sample 12 (S12) has a few more millimeters to go till the cork which in this case is considered as full compression, thus by the above-mentioned reasoning we will be measuring performance in different cases which is not a fair comparison. For proper comparison of different brands, one should measure the force at full compression. A better way is to express displacement as percentage compression defined as [(produced displacement)/(max possible displacement) x 100] or [E/D x100] as shown in figure3.40, this way we would non denationalise the displacement parameter and comparison between any samples will be possible.

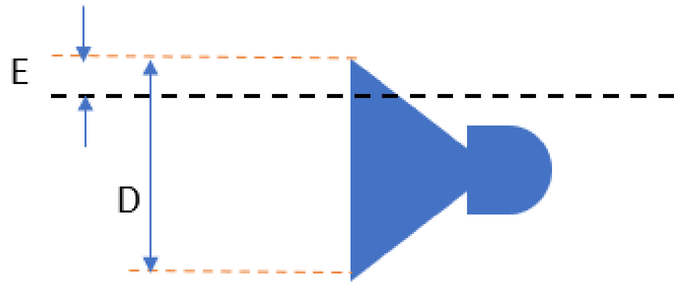

Figure 3.40: Schematic representation of shuttle dimensions

The data obtained from the first trial of the modified compression test is shown in fig 3.41, the general trend of the graph is that the resistance load increases exponentially with displacement, thus the higher the % compression used for comparison of the samples the more significant the difference appear. In the previous method comparison was only possible till displacements where the disc struck the cork while in this method loads at much further displacements can be compared giving higher accuracy of comparison. In the plot it can be seen that the load suddenly drops from its usual trend and then spikes again, this point of dip indicates the point where the feather root started tearing away from the root. This can give faulty comparison thus requiring additional modification to the test.

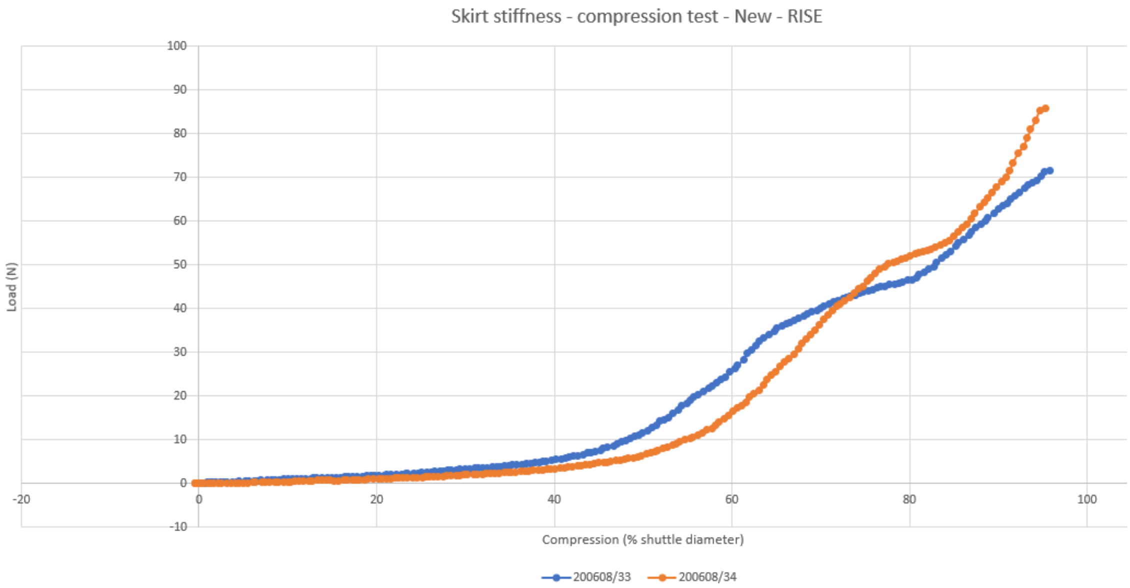

Figure 3.41: Results from modified skirt compression test

3.2.2.3 Comparison of skirt stiffness results

To validate the smash rig the data from conventional skirt compression data for the machine smashed samples were compared to the data of player smashed shuttles from the same brand, it is to be noted that the conventional skirt compression test even though discarded is still valid for comparison between same brands or samples and hence this validation is reliable. The comparison data is shown in table 3.41, it shows that the damage from machine and player were similar for Yonex shuttles and since this was the reference brand it was concluded that the mechanism has achieved its goal in replication real life smashes.

Smash test		New shuttle					New shuttle					
	Monitoring in Nov 2019 Reference for player smash	Loads in N for Deformation (mm)				Monitoring in Nov 2020 Reference for machine smash	Loads in N for Deformation (mm)			% difference in load for deformation in mm		
	Brands	15	25	35		Brands	15	25	35	15	25	35
815	RCL Black Silver	2.4	5.6	25.4	815	RCL Black Silver	2.2	5.9	23.8	-9.99968164	5.576591343	-6.315706
819	Tour Dragons Brand 5 Sports	2.3	5.3	31.2	819	Tour Dragon Brand 5 Sports	1.9	4.7	26.9	-17.53499544	-11.00833424	-13.87717
887	Yonex Tournament	2.1	5.3	26.4	887	Yonex Aerosensa F-90	2.3	5.3	25.1	7.44642403	0.334206786	-5.000426

Smash test		used shuttle					used shuttle					
	Monitoring in Nov 2019 player smashed	Average used shuttle				Monitoring in Nov 2020 machine smashed	Average used shuttle			% difference in load for deformation in mm		
	Brands	15	25	35		Brands	15	25	35	15	25	35
815	RCL Black Silver	2.0	4.6	17.5	815	RCL Black Silver	1.70	3.70	12.50	-15	-19.56521739	-28.57143
819	Tour Dragons Brand 5 Sports	1.8	4.4	28.3	819	Tour Dragon Brand 5 Sports	1.50	3.40	17.00	-16.66666667	-22.72727273	-39.92933
887	Yonex Tournament	1.8	4.1	18.1	887	Yonex Aerosensa F-90	1.7	4.4	21.9	-5.555555556	7.317073171	20.99448

Figure 3.42: Comparison of conventional skirt compression test results for player smashed and machine smashed samples

For two brands other than Yonex the smash resistance showed notable variation between samples of the same brand smashed by a player and by the machine. This was assumed to be caused by two reasons. Due to the variation of mechanical properties within the shuttlecock it is possible that a given sample could have different damage resistance in different radial directions, thus giving different results when smashed on different feathers.

Another reason is assumed to be due to the presence of large variation in properties within samples of the same tube, this is partially evident from the above table where by comparing the reference shuttles of 2019 and 2020 despite being samples from the same brand, a significant % difference in loads can be observed for 819. However these reasons need to be further investigated.

3.2.3 Shuttlecock velocity

Based on the feed back from Mr.Christer that the shuttle changes speed (usually flies faster) after damage usually within the first two meters of flight, It was decided to monitor the change in shuttle velocity as the smash test progressed to quantify the damage. The shuttle velocity was measured at a fixed distance of 1.5 m from the contact point at subsequent smash intervals, a slow motion footage was captured and analysed for every first, fifth, tenth and fifteenth smash per sample. The data obtained is listed in figure 3.43 the velocity was observed to change marginally and randomly, thus showing that this approach was not feasible. Parallel to shuttle velocities racket velocities were also measured to make sure that initial conditions were same for all shuttle smashes, from this data it was observed that the racket produced consistent smash speeds of about 43 m/s ensuring repeatability of the mechanism.

Sl. num	Brand	Sample num	Smash num	Marker velocity (V1)	(R2/R1)	Racket tip vel (V2)	Avg Racket tip vel	Shuttle Velocity	velocity difference	Avg Shuttle vel per smash per brand
				m/s		m/s	m/s	m/s	m/s	m/s
1	Yonnex - 887	1	1	30.0596	1.452380952	43.65799048	43.06859008	42.5597		42.82346667
2			5	28.4307	1.452380952	41.29220714		43.6909	1.1312	41.3235
3			10	30.3968	1.452380952	44.14773333		44.377	0.6861	42.73656667
4			15	28.4935	1.452380952	41.38341667		43.9539	-0.4231	42.431
5		2	1	28.9632	1.452380952	42.0656		43.7344		
6			5	27.9622	1.452380952	40.61176667		38.0728	-5.6616	
7			10	29.2741	1.452380952	42.51714524		41.5481	3.4753	
8			15	29.1211	1.452380952	42.29493095		41.0748	-0.4733	
9		3	1	30.1409	1.452380952	43.77606905		42.1763		
10			5	28.953	1.452380952	42.05078571		42.2068	0.0305	
11			10	29.1629	1.452380952	42.35564048		42.2846	0.0778	
12			15	30.4375	1.452380952	44.20684524		42.2643	-0.0203	
13	819	1	1	29.9662	1.452380952	43.5223381		45.1152		45.38833333
14			5	30.0181	1.452380952	43.59771667		44.1501	-0.9651	45.30756667
15			10	30.1552	1.452380952	43.7968381		45.7952	1.6451	45.36563333
16			15	28.9433	1.452380952	42.03669762		44.662	-1.1332	45.14333333
17		2	1	30.0219	1.452380952	43.60323571		45.0928		
18			5	30.1552	1.452380952	43.7968381		46.4736	1.3808	
19			10	29.7575	1.452380952	43.21922619		45.6178	-0.8558	
20			15	30.066	1.452380952	43.66728571		45.45	-0.1678	
21		3	1	29.9275	1.452380952	43.46613095		45.957		
22			5	29.9767	1.452380952	43.5375881		45.299	-0.658	
23			10	30.1086	1.452380952	43.72915714		44.6839	-0.6151	
24			15	29.5004	1.452380952	42.84581905		45.318	0.6341	
25	815	1	1	30.0259	1.452380952	43.60904524		41.7058		41.4386
26			5	29.7129	1.452380952	43.15445		41.4296	-0.2762	41.4525
27			10	30.2216	1.452380952	43.89327619		41.6202	0.1906	41.862
28			15	29.6895	1.452380952	43.12046429		40.1499	-1.4703	40.49143333
29		2	1	29.0829	1.452380952	42.23945		41.7058		
30			5	30.3779	1.452380952	44.12028333		41.4296	-0.2762	
31			10	30.3791	1.452380952	44.12202619		41.6202	0.1906	
32			15	28.9632	1.452380952	42.0656		40.1499	-1.4703	
33		3	1	29.554	1.452380952	42.92366667		40.9042		
34			5	30.2561	1.452380952	43.94338333		41.4983	0.5941	
35			10	30.3497	1.452380952	44.07932619		42.3456	0.8473	
36			15	28.9313	1.452380952	42.01926905		41.1745	-1.1711	

Figure 3.43: Machine smash test results of 887, 815 and 819 with three samples each

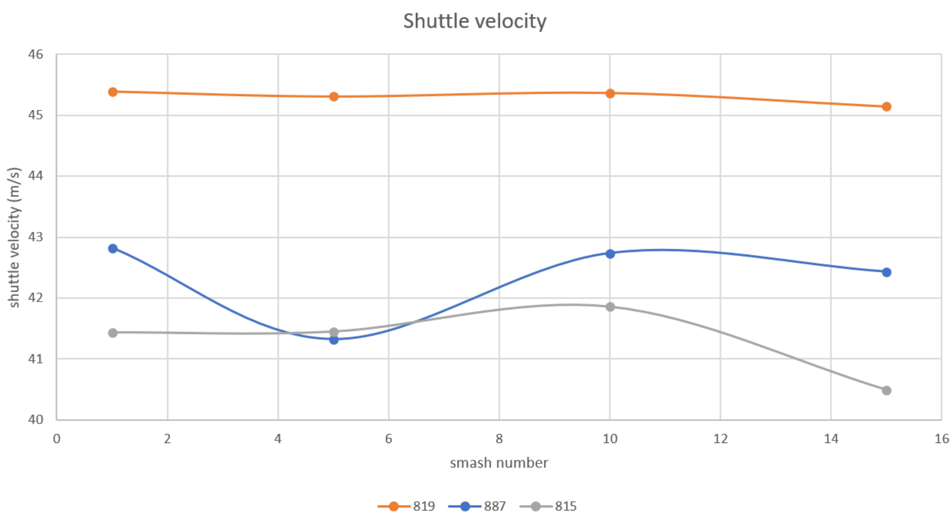

Figure 3.44: Change in the average velocities of the samples over the smashes

3.2.3.1 Player Test

an investigation into the kinematics of shuttlecock smash motion [5] revealed that the horizontal distance travelled by the shuttle 'X' is related to the square of its terminal velocity 'V_t' (refer equation 3.14). When the shuttle gets damaged its aerodynamic properties changes and hence its terminal velocity changes but since monitoring velocity was proven to be difficult it was decided to monitor the distance as this indirectly measures 'V_t', also due to the square relation the difference in 'X' will show a magnified difference in 'V_t'.

$$X = \frac{V_t^2}{g} \ln \left[\frac{V_{xi}gt + V_t^2}{V_t^2} \right] \tag{3.14}$$

This approach was tested with a professional player in a real court, the player was placed on the intersection of the court lines as shown in figure 3.45, he was asked to smash a given shuttle 10 times with the same force and at same height, the shuttle was smashed straight and parallel to the ground (at 0 deg launch angle). The distance along Y is measured for the first and final smashes and the difference in distance were noted.

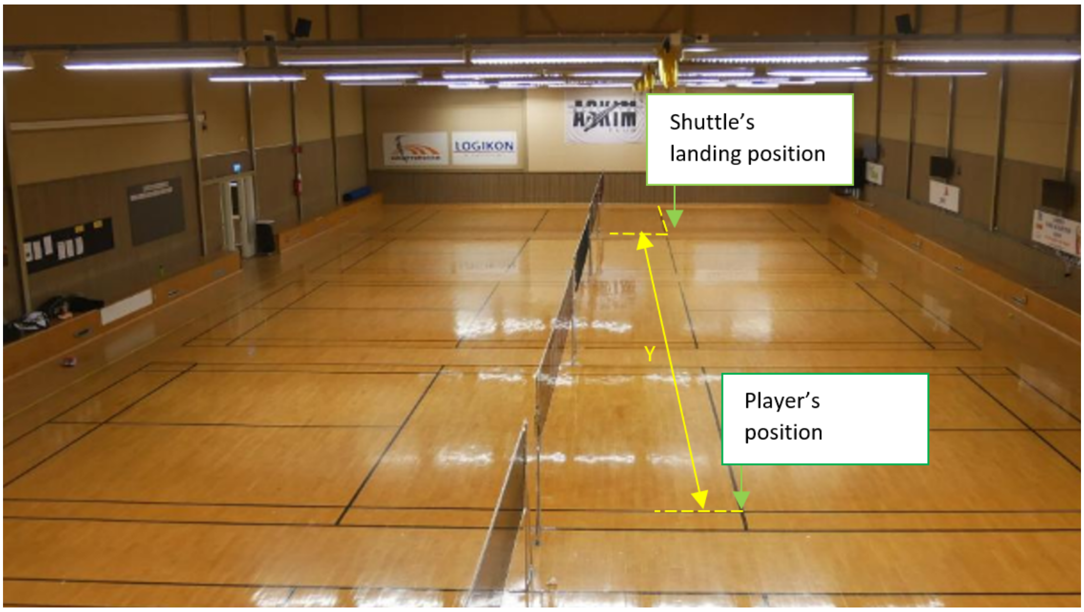

Figure 3.45: Change in the average velocities of the samples over the smashes

12 brands were tested and their results have been tabulated in 3.46. A measurable difference in displacement was observed after damage for all brands. Thus distance measurement was a more reliable test method for damage detection, this method also directly shows the performance of the shuttle in a game unlike in skirt compression test making it more ideal. Due to these reasons it was decided to implement this approach future experiments.

May 2020	**Difference in flight distance before and after smash test (10 strokes)**					
Badminton Shuttlecock Characterization test						
Brand		Before smash, cm from baselin	After smash, c	Difference (c	Conclusion	Comment
900	FZ Forza VIP	120	60	60	Faster	Slow shuttle
901	Oliver APEX 200	130	45	85	Faster	Slow shuttle
902	LiNing 600+	55	75	-20	Slower	
903	Aero-flight 800 Supergrade	45	20	25	Faster	Fast shuttle
904	Adidas FS7	40	35	5	Faster	Fast shuttle
905	Kawasaki No 1	60	75	-15	Slower	
906	Ling-mei	70	50	20	Faster	
907	Victor Gold Champion	65	50	15	Faster	
908	CHAO-PAI	45	30	15	Faster	Fast shuttle
909	MMOA Super Select	75	5	70	Faster	
910	Jinque AAA	140	120	20	Faster	Slow shuttle
911	FBT	120	100	20	Faster	Slow shuttle
842	Yonex Tournament 1	95	85	10	Faster	
842	Yonex Tournament 2	90	80	10	Faster	
842	Yonex Tournament 3	90	50	40	Faster	

Figure 3.46: Change in the average velocities of the samples over the smashes

3.3 Tumble Rig Improvements

3.3.1 Previous Test Rig and Limitations

The previous tumble test rig even though produced realistic tumbling, it lacked repeatability as the amount of tumble and the final landing position of the shuttle was observed to show significant variance.

3.3.2 New Rig Mechanism and Theory

As explored in the previous phase tumble can be produced by multiple ways, but in this case the simplest movement was selected in which the racket held at an angle is accelerated horizontally towards the approaching shuttlecock striking it at an angle which produces a spin and also bounces it back into the opposite court.

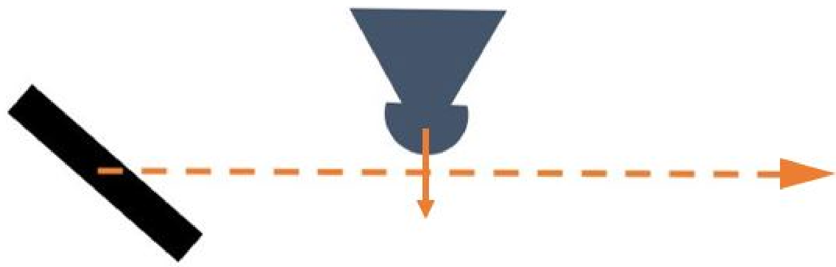

Figure 3.47: Front view of the experimental set up for replicating tumble from the racket Reference Frame.

Based on the same principle of relative velocity as employed in the previous phase of tumble test rig development, complex movements of falling shuttle and approaching racket can be simplified into shuttle being held stationary and the racket accelerating towards it at an angle.

The new tumble mechanism consists of a long rail or 44mm x44mm flex link called the sliding rail bolted to two other vertical rails refer figures 3.48 and 3.49, this provides two points of fixture which was shown to be necessary to resist all moments and avoid slippage. The bolting points on the two rails can be altered making it possible to fix the sliding rail at the required height and angle. On the front end of the sliding rail a smaller flex link member is bolted firmly in place and a spring is attached to it. The other end of the spring is attached to a similar short flex link known as the travelling member which can slide freely on the sliding rail, two Teflon legs align the travelling member to the groove on the rail, the Teflon legs also reduce sliding friction so that the member can travel with ease. Using a short flex link and an angle joint an offset arm which can be aligned at the desired angle is fixed to the moving member and the racket is fixed to this member. The shuttlecock is held in position by the same vacuum and straw mechanism used so far, the straw is fixed to a flex link member which can move all three axes thus being able to align the shuttle anywhere in space such that the shuttle always strikes the racket center as shown in figures 3.50 and 3.51.

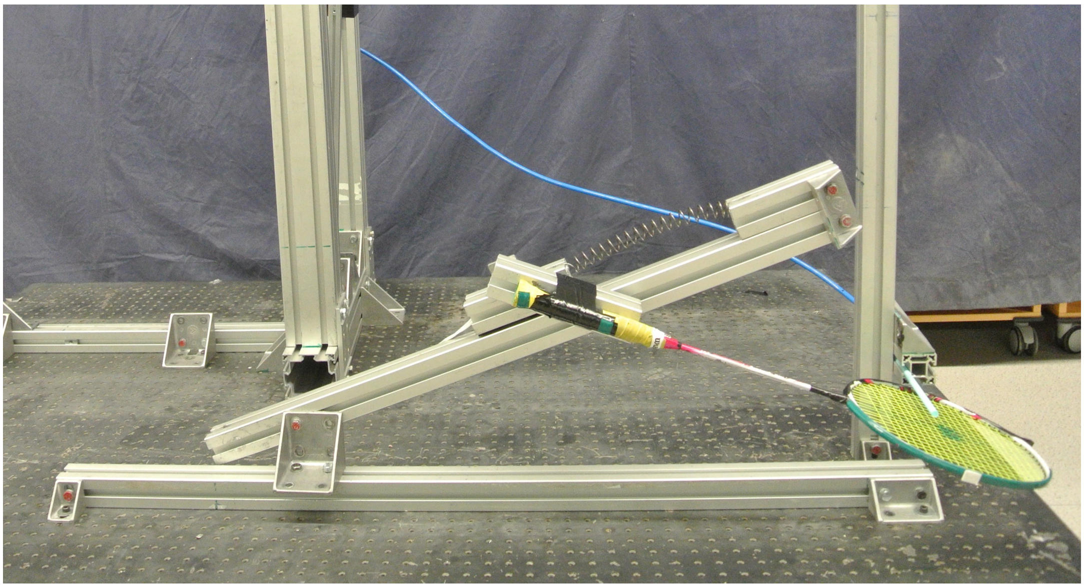

Figure 3.48: New tumble mechanism - iso view.

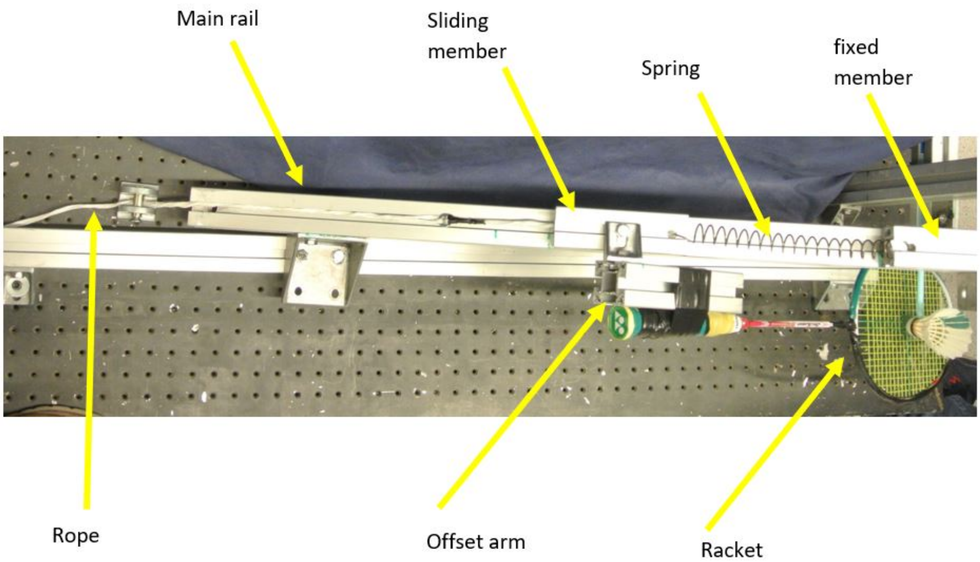

Figure 3.49: New tumble mechanism - top view.

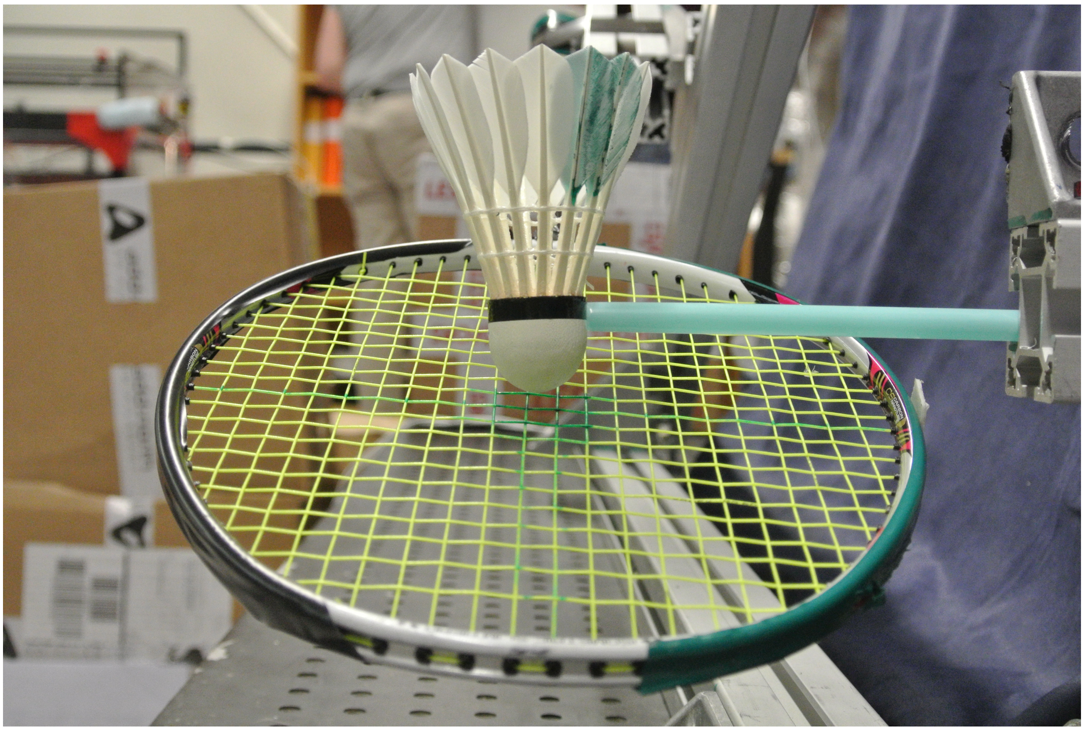

Figure 3.50: Front view of the shuttle position upon impact with the racket.

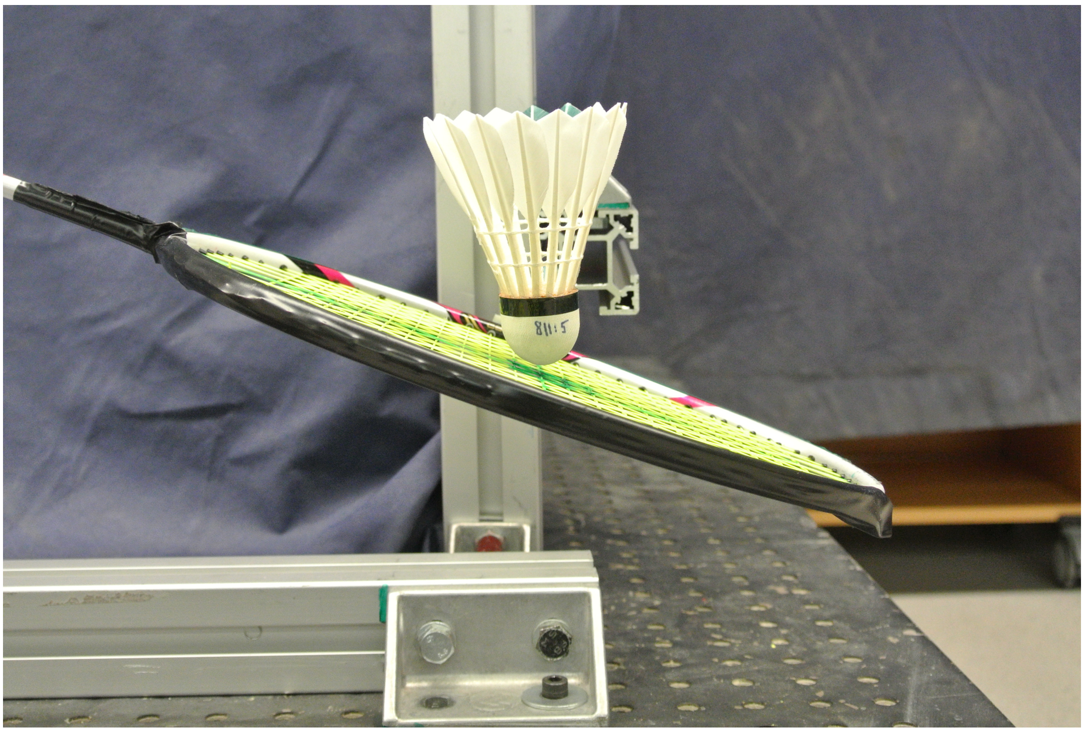

Figure 3.51: Side view of the shuttle position upon impact with the racket.

3.3.3 experimental Setup

The experimental facility is setup as shown in the figure 3.52, The test rig mounted firmly on a rigid base so as reduce slips and vibrations, a camera is placed at right angles such that the video frame is parallel to the plane of motion of the moving member and a dark screen (made of cloth) is used as background for the video recording.

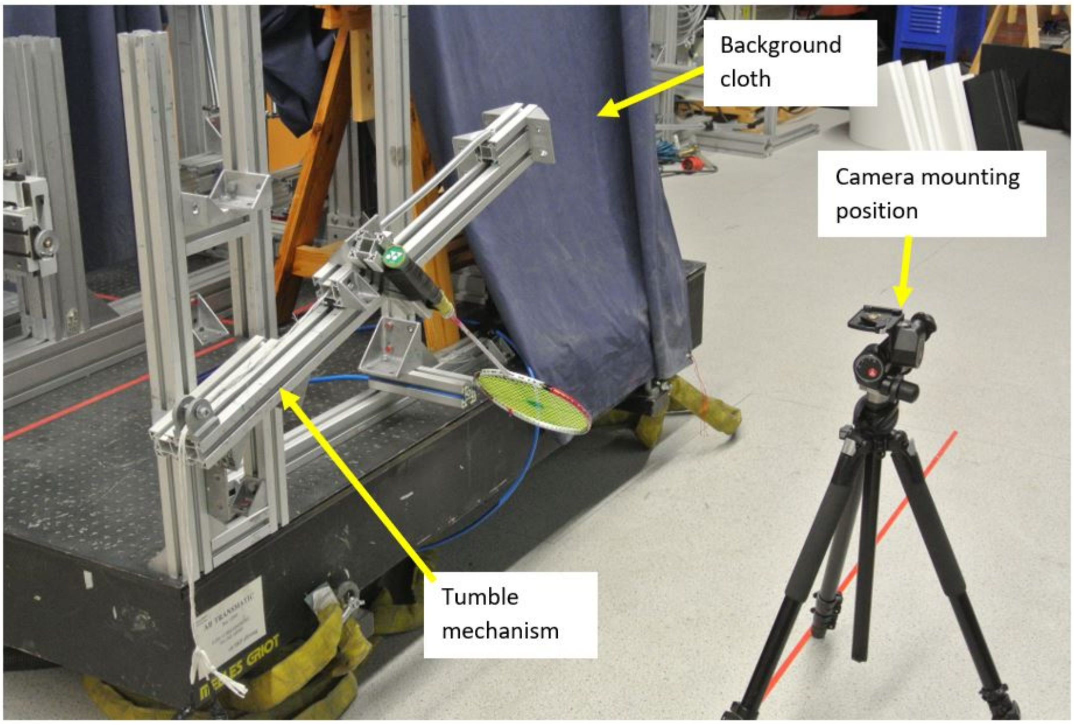

Figure 3.52: Tumble test experiment setup.

To replicate tumble the sliding rail is aligned at the required position and orientation followed by aligning racket on the moving member. the shuttlecock in positioned in space such that it strike the racket at the required position, also the shuttle orientation is adjusted to a prescribed angle in the vertical plane. Once the setup is ready the moving member is pulled back with the help of a rope attached to it, this action stretches the spring and loads the mechanism. Once the camera is ready the rope is released and the racket is set in motion, it strikes the shuttle and creates tumble which is recorded and post processed

The Camera used is a Nikon 1 model which can capture 400 Frames per second at 640x480 pixels resolution and for post processing PCC 3.4 is used.

3.3.4 Initial Trials

For primary validation of the test rig five shuttlecocks as shown in the figure 3.53 were chosen which included both feathered and synthetic shuttlecocks. One sample from four brands which are factory manufactured were used and one shuttle was created by removing alternate feathers and driving a nail inside the cork. Since the relative tumbling performance of these shuttlecocks were known they were used to validate the performance of the rig.

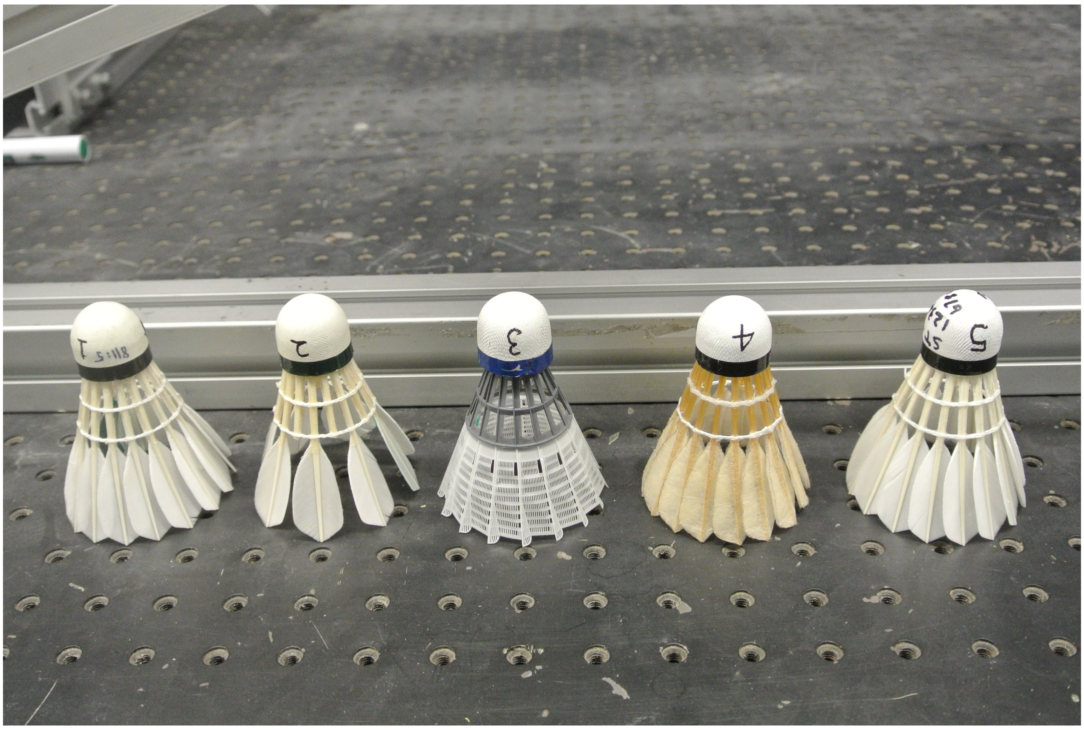

Figure 3.53: Test samples used for primary validation of the tumble test rig.

From the experiments it was observed that 'S4' produced the maximum amount of tumble and 'S2' produced the least, this was in agreement with previous observations hence showing that the test rig produces realistic results. Tumble was measured as the number of revolutions the shuttlecock performed in the plane parallel to the camera frame. The amount of tumbles for different samples are listed in table 3.54. A difference in tumble was also observed between all brands with a minimum difference of 0.25 revolutions and a maximum of 0.75 revolutions, difference between all the samples are listed in the table3.55.

SAMPLE	TUMBLE
S1	2
S2	1.5
S3	2.25
S4	2.5
S5	1.75

Figure 3.54: Observations from the primary validation of the tumble test.

		S1	S2	S3	S4	S5
		2	1.5	2.25	2.5	1.75
S1	2	0	-0.5	0.25	0.5	-0.25
S2	1.5	0.5	0	0.75	1	0.25
S3	2.25	-0.25	-0.75	0	0.25	-0.5
S4	2.5	-2.75	-1	-0.25	0	-0.75
S5	1.75	0.25	-0.25	0.5	0.75	0

Figure 3.55: The matrix showing differences in tumbles between each samples.

3.3.5 Optimization

Even though the tumble amount was observed to be realistic feedback from Mr.Christer suggested that the absolute amount of tumble was found to be less than that observed in reality. Thus it was decided to modify the rig parameters and maximize the tumble.

3.3.5.1 Setup

To optimize the rig the base line brand of shuttle used was S2, the reasoning behind which was that since this shuttle had the most tendency to tumble, it would highlight the influence of parameters on tumble.

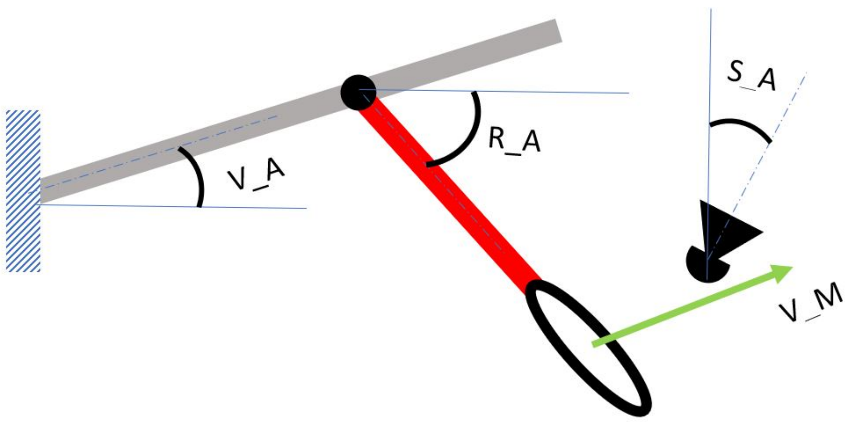

Figure 3.56: Tumble test rig schematic diagram with illustrated parameters.

The rig consists of four independent parameters as shown in figure 3.57. These are: the velocity angle 'V_A or the angle made by the main rail with the horizon, this quantity is controlled by the two bolting position of the main rail. The racket angle 'R_A or the angle made by the racket with the horizon, adjusted by changing the angle of the offset arm attached to the moving member. The shuttle angle S_A or the angle made by the shuttle with the vertical axis which can be adjusted by simply attaching the shuttle to the straw at the required angle and finally the velocity magnitude V_M or the speed at which racket strikes the shuttle, which is adjusted by adjusting the amount of stretching of the spring when loading the mechanism. The response measured in the experiment is the amount of tumble.

It is required to test as much combination of these parameters to find the optimum settings which can be a huge number of tests. In order to reduce the total number of tests an optimization methodology known as response surface method was employed, this method stems from the field of Design of experiments which studies methods of extracting maximum amount of useful information from minimum number of experiments, the software JMP Pro 14 was used for the design of the experiments and post processing of the data .

The sample space of tests was defined by the following range of parameters which were set arbitrarily based on previous observations and real game footage. V_M from spring settings 1 to 2, S_A from 0 degrees to 40 degrees, R_A from 0 degrees to 30 degrees and V_A from 30 degrees to 60 degrees

A Central Composite design was used, this method only requires two levels of each factor at the far ends of the sample space greatly reducing the number of tests. In addition a Rotatable design was also chosen, this method gives uniform prediction variance across the sample space which avoids any bias towards a particular region in the sample space giving fair predictions. The calculated number of tests/runs were 26 however frequent analysis of the data during experimentation showed that the model acquired a good fit after 22 runs.

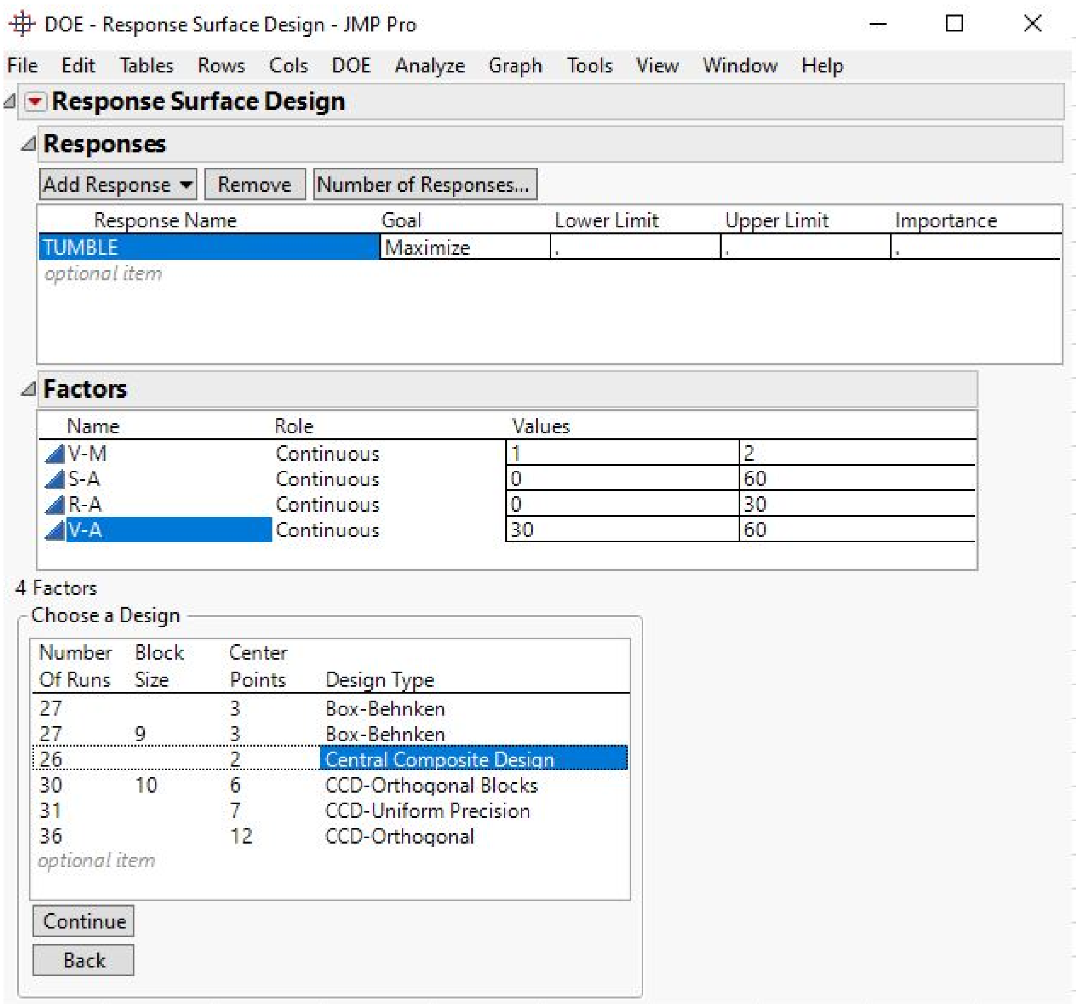

Figure 3.57: Design of experiment setup in JMP pro 14.

3.3.6 Validation

The results from the 22 runs are tabulated in table 3.58, JMP Pro uses this data to build a regression model to predict the optimum settings, to see if the regression model produced is reliable it is mandatory to check the fit characteristics of the data which include checking the RSq (R Squared) values calculated, as can be seen from figure 3.59 the RSq value is close to 1 which indicates a good fit and hence the model is reliable for predictions [6].

Pattern	V-M	S-A deg	R-A deg	V-A deg	TUMBLE deg		V - R - A deg	R-S-A deg		TUMBLE revs
−−+−	1	0	30	30	540		60	60		1.5
++−+	2	40	0	60	365		60	130		1.013889
+−+−	2	0	30	30	855		60	60		2.375
−−−+	1	0	0	60	405		60	90		1.125
++++	2	40	30	60	360		90	100		1
−−−−	1	0	0	30	405		30	90		1.125
0	1.5	20	15	45	425		60	95		1.180556
00a0	1.5	20	-15	45	425		30	125		1.180556
000a	1.5	20	15	15	295		30	95		0.819444
0	1.5	20	15	45	425		60	95		1.180556
+−++	2	0	30	60	720		90	60		2
a000	0.5	20	15	45	45		60	95		0.125
−+−+	1	40	0	60	225		60	130		0.625
+−−−	2	0	0	30	765		30	90		2.125
−+−−	1	40	0	30	180		30	130		0.5
−++−	1	40	30	30	270		60	100		0.75
+−−+	2	0	0	60	765		60	90		2.125
0a00	1.5	-20	15	45	790		60	55		2.194444
+++−	2	40	30	30	445		60	100		1.236111
00A0	1.5	20	45	45	360		90	65		1
−+++	1	40	30	60	365		90	100		1.013889
++−−	2	40	0	30	500		30	130		1.388889

Figure 3.58: Table of runs.

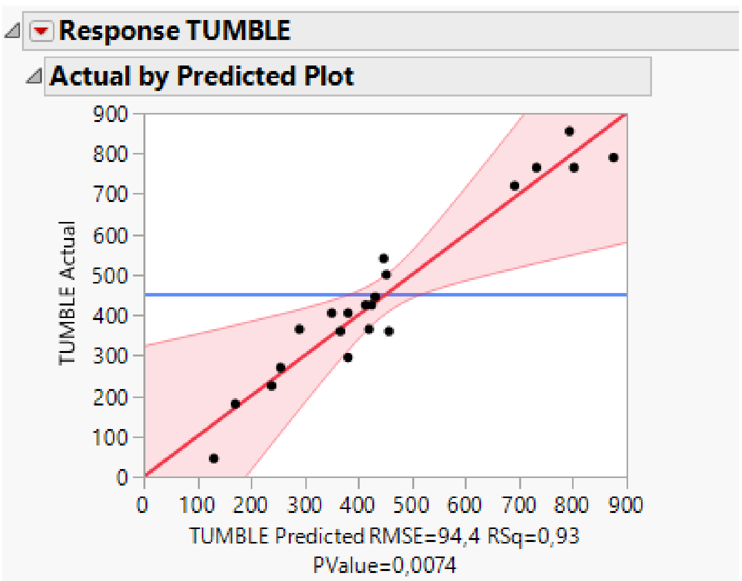

Figure 3.59: Fit diagram.

The influence of each parameter or a combination of them can also be derived from the data, for understanding this we look at the P value chart as shown in the figure 3.60, a lower p value shows higher influence, thus in this case it can be seen that the velocity magnitude has the highest influence on tumble followed by shuttle angle.

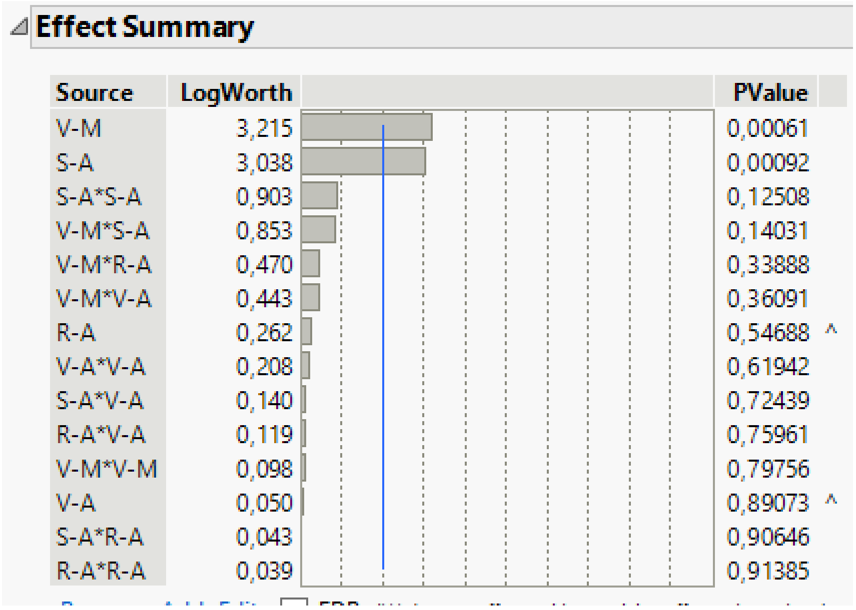

Effect Summary

Source	LogWorth	PValue	
V-M	3,215	0,00061	
S-A	3,038	0,00092	
S-A*S-A	0,903	0,12508	
V-M*S-A	0,853	0,14031	
V-M*R-A	0,470	0,33888	
V-M*V-A	0,443	0,36091	
R-A	0,262	0,54688	^
V-A*V-A	0,208	0,61942	
S-A*V-A	0,140	0,72439	
R-A*V-A	0,119	0,75961	
V-M*V-M	0,098	0,79756	
V-A	0,050	0,89073	^
S-A*R-A	0,043	0,90646	
R-A*R-A	0,039	0,91385	

Figure 3.60: P value chart.

Finally using the software the optimum conditions to maximize the tumble is predicted as shown in figure 3.61 and these turns out to be when the man rail is at 15 degree, the racket is tilted 45 degrees, shuttle is titled 20 degrees towards the racket and the spring is set at position 2. The maximum amount of tumble predicted by the model for sample S2 was 1152.856 degrees of rotation which turns out to be 3.202 revolutions. Testing the rig with the optimum setting showed that S2 produced about 3.125 revolutions which was close to the predicted number. This amount of tumble was observed to be realistic and hence concluded that further optimization was not necessary. The tumbles were also found to be very repeatable which is a great advantage compared to mechanisms developed in the previous phase. The same sample S2 was tested 10 times at a random setting and it was shown that deviations only occurs 2 times which was also due to human errors. The results from the repeatability test are listed in the table **??**

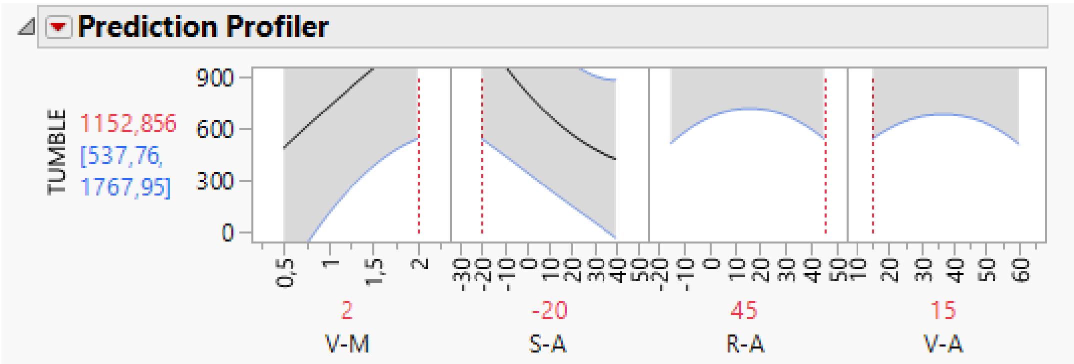

Figure 3.61: prediction profile showing optimum settings.

SL.NUM	V-M	S-A	R-A	V-A	TUMBLE	AVG TUMBLE	% ERROR	MAX ERROR	REMARK
1	2	0	0	60	2.17	2.136	-1.5917603	6.4	repeatable max error in some exp is due to rope slippage which was human error
2	2	0	0	60	2.17	2.136	-1.5917603		
3	2	0	0	60	2.17	2.136	-1.5917603		
4	2	0	0	60	2.17	2.136	-1.5917603		
5	2	0	0	60	2	2.136	6.367041199		
6	2	0	0	60	2.17	2.136	-1.5917603		
7	2	0	0	60	2.17	2.136	-1.5917603		
8	2	0	0	60	2.17	2.136	-1.5917603		
9	2	0	0	60	2	2.136	6.367041199		
10	2	0	0	60	2.17	2.136	-1.5917603		

Figure 3.62: Results from repeatability tests.

3.4 Final Test Results

For the final validation of the tumble test rig, 7 brands of shuttlecocks as shown in figure 3.63 were tested at optimum settings and their results were compared.

Figure 3.63: Final tumble test samples

During the test it was noted that some shuttlecocks revolved quite quickly which led the skirt of the shuttle to crash onto the racket string bed, this stopped the shuttles from undergoing full tumble and a wrong value of tumble was measured. To counteract this problem the shuttle angle was increased from -20 to 20 degrees so that the shuttles get enough room to rotate and will miss the string bed as they fly away, however increasing the shuttle angle would reduce the tumble as observed from the regression model, this was compensated by increasing the racket velocity and the spring were stretched to maximum. The final result of these modifications was that the shuttle produced interference free tumble which exceed the previous optimum by a small margin.

Three specimen from each brand were randomly chosen and tested and the average tumble from each brand were noted. The results from the final test are listed in the table 3.64

SL NUM	BRAND NUM - TYPE	SAMPLE NUM							Total num of revs	avg revs per brand
			deg	number of revs	remark	deg	number of rotations	remark	revs	revs
1		1	930	2.583333333	normal	205	0.569444444	G	3.152777778	
2	865 - SYNTHETIC	2	930	2.583333333	normal	205	0.569444444	G	3.152777778	
3		3	930	2.583333333	normal	205	0.569444444	G	3.152777778	3.152777778
4		1	390	1.083333333	normal	200	0.555555556	R	1.638888889	
5	547 - FEATHERED	2	390	1.083333333	normal	200	0.555555556	R	1.638888889	
6		3	775	2.152777778	normal	45	0.125	G	2.277777778	1.851851852
7		1	775	2.152777778	normal	105	0.291666667	G	2.444444444	
8	887 - FEATHERED	2	580	1.611111111	normal	210	0.583333333	R	2.194444444	
9		3	580	1.611111111	normal	210	0.583333333	R	2.194444444	2.277777778
10		1	595	1.652777778	normal	135	0.375	G	2.027777778	
11	819 - FEATHERED	2	570	1.583333333	normal	210	0.583333333	R	2.166666667	
12		3	595	1.652777778	normal	135	0.375	G	2.027777778	2.074074074
13		1	940	2.611111111	normal	180	0.5	G	3.111111111	
14	827 - SYNTHETIC	2	940	2.611111111	normal	180	0.5	G	3.111111111	
15		3	955	2.652777778	normal	135	0.375	G	3.027777778	3.083333333
16		1	890	2.472222222	normal	160	0.444444444	G	2.916666667	
17	H - PLASTIC	2	890	2.472222222	normal	160	0.444444444	G	2.916666667	
18		3	890	2.472222222	normal	160	0.444444444	G	2.916666667	2.916666667
19		1	850	2.361111111	normal	120	0.333333333	G	2.694444444	
	815 - FEATHERED	1	850	2.361111111	normal	120	0.333333333	G	2.694444444	
		1	850	2.361111111	normal	120	0.333333333	G	2.694444444	2.694444444

Figure 3.64: Final tumble test observation table

It was interesting to note that the tumbling process was not perfectly planar or uni axial, in some cases the shuttle would reverse the spin in mid flight, other times the shuttles would spin around more than one axis with majority of the spin in the observation plane. Only spins in the plane of observations were noted and both forward and backward spins were counted.

It was noted that in general Synthetic and Plastic shuttles tumbled more than the feathered ones which has been previously observed, this can be seen from the bar chart 3.65 which compares the average tumbles between the different brands

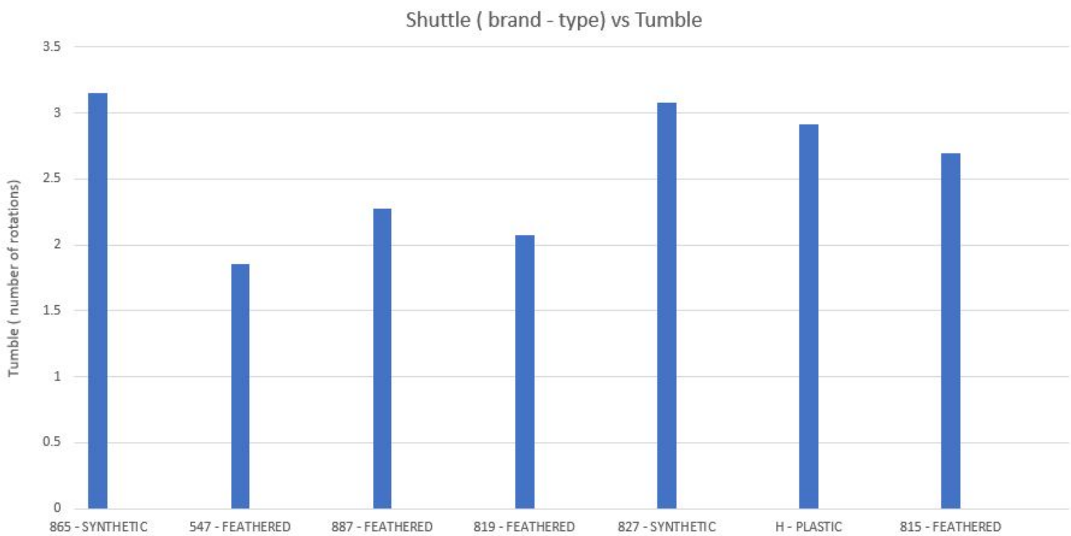

Figure 3.65: Final tumble test observation table

Deviation in tumbles between samples of the same brand were compared and it was observed that the the tumbles were more consistent between samples of synthetic and plastic brands compared to feathered ones.
Deviation of average tumble between brands were also calculated and it showed that deviation is more between feathered brands compared to synthetic or plastic ones.

The table 3.66 reveals this data sorted in ascending order. A minimum difference of about 25 degrees and a maximum difference of about 1.3 revolutions was observed.

SL NUM	BRANDS	TUMBLE	BRANDS	TUMBLE	DIFFERENCE IN TUMBLE		ABS VALUE
		rotn		rotn	rotn	deg	deg
1	827_S	3.083	865_S	3.152	0.069	24.84	24.84
2	H_P	2.916	827_S	3.083	0.167	60.12	60.12
3	819_F	2.074	887_F	2.277	0.203	73.08	73.08
4	815_F	2.694	H_P	2.916	0.222	79.92	79.92
5	819_F	2.074	547_F	1.851	-0.223	-80.28	80.28
6	H_P	2.916	865_S	3.152	0.236	84.96	84.96
7	815_F	2.694	827_S	3.083	0.389	140.04	140.04
8	887_F	2.277	815_F	2.694	0.417	150.12	150.12
9	547_F	1.851	887_F	2.277	0.426	153.36	153.36
10	865_S	3.152	815_F	2.694	-0.458	-164.88	164.88
11	815_F	2.694	819_F	2.074	-0.62	-223.2	223.2
12	H_P	2.916	887_F	2.277	-0.639	-230.04	230.04
13	827_S	3.083	887_F	2.277	-0.806	-290.16	290.16
14	H_P	2.916	819_F	2.074	-0.842	-303.12	303.12
15	815_F	2.694	547_F	1.851	-0.843	-303.48	303.48
16	887_F	2.277	865_S	3.152	0.875	315	315
17	827_S	3.083	819_F	2.074	-1.009	-363.24	363.24
18	H_P	2.916	547_F	1.851	-1.065	-383.4	383.4
19	819_F	2.074	865_S	3.152	1.078	388.08	388.08
20	827_S	3.083	547_F	1.851	-1.232	-443.52	443.52
21	547_F	1.851	865_S	3.152	1.301	468.36	468.36

Figure 3.66: Table of difference in average tumbles between brands

Feedback of the test results from Mr.Christer suggested that it was preferred to increase the tumbles of each brand as much as possible inorder to highlight the difference between brands leading to easy comparison. Thus further modifications will be made to the rig such as changing the spring to further increase the tumble.

4
Conclusion and Future work

The smash rig from the previous iteration was rebuilt to a high-power fully functioning and repeatable test rig. The analysis of slow-motion footage from 36 smashes showed that the mechanism produced consistent smash speed of above 40 m/s which is well within the recommended limit suggested by previous studies. The test rig was used for smashing a set of 9 shuttlecock samples from 3 brands (3 samples per brand) 15 times “on the same feather” (mounting the shuttlecock in same position at each smash), after which the samples were subjected to the standard skirt compression test by Polyfor. The obtained data for a machine smashed Yonex shuttlecock was compared to the data from a player smashed Yonex shuttlecock and good agreement of the results was found.

For two brands other than Yonex the smash resistance showed notable variation between samples of the same brand smashed by a player and by the machine. This was assumed to be caused by the variation of mechanical properties within the shuttlecock giving different damage resistance in different radial directions. Another reason for observed variation maybe to be due to the presence of large variation in properties within samples of the same tube, this was partially evident from the compression test data. However these reasons needs to be further investigated along with testing of more samples (especially synthetic) and an allowable range of difference in performance must be defined.

To check for variations the following methodology was proposed - 12 shuttles from a tube are to be divided into four groups of three shuttles each. The first group will be an untouched reference, the second group will be tested by players, the third group will be tested in the machine, and the fourth group will be tested in the machine but the shuttles will be rotated by 1/16 turn for every smash. Before the tests, “face side” are marked for all the shuttles and compression tests from this side (for all 12) before and after smashing will be performed at Polyfor.

For replicating tumble, a new tumble test rig design was build, optimised and validated. From a series of 10 tests the rig proved to be repeatable, amount of tumble was also observed to be realistic from a set of 22 tests and produced notable difference between feathered and synthetic shuttles. However the smallest difference was measured to be 25 degrees which was deemed as marginal, thus difference must be increased further. During the tumbling process the revolutions of the shuttle was observed to be occur in around 3 axes to measure all the revolutions the current setup must be modified from one camera to two perpendicular cameras. The tumbling tests for several brands, types (especially for synthetic), and batches of shuttles also have to be performed.

The current skirt compression method is an indirect measurement of the shuttlecock's performance in a real game. Also compressing a shuttlecock prior to a smash test to derive its baseline smash resistance partially damages it in one direction, which could affect the compression test results after the smash test if it is smashed again in this direction. Furthermore, the test is blind to the effects of rumpling. For these reasons, other possible methods of measuring the effect of smash damage were looked into, these included monitoring the flight distance directly or monitoring the terminal velocity of the shuttle from wind tunnels or drop tests. These methods have to be tested and if found to be effective could potentially replace the current test method used by Polyfor.

References

[1] (accessed:10.5.2020) Hooke's law. [Online]. Available: https://en.wikipedia.org/wiki/Hookes_law

[2] T. Helmenstine. (accessed:7.5.2020) Hooke's law example problem - worked example problems. [Online]. Available: https://sciencenotes.org/hookes-law-example-problem/

[3] (accessed:6.5.2020) Rotational energy. [Online]. Available: https://en.wikipedia.org/wiki/Rotational_energy

[4] (accessed:5.5.2020) list of moments of inertia. [Online]. Available: https://en.wikipedia.org/wiki/List_of_moments_of_inertia

[5] L.-M. Chen, Y.-H. Pan, and Y.-J. Chen, "A study of shuttlecock's trajectory in badminton," *Journal of sports science & medicine*, vol. 8, no. 4, p. 657, 2009.

[6] (accessed:5.5.2020) interpreting regression results 2020. [Online]. Available: https://www.jmp.com/en_us/statistics-knowledge-portal/what-is-regression/interpreting-regression-results.html